A comprehensive discovery platform for ELOVL1 small-molecule inhibitors targeting very long-chain fatty acid synthesis in adrenoleukodystrophy

Received for publication, November 23, 2025, and in revised form, April 16, 2026 Published, Papers in Press, May 6, 2026
https://doi.org/10.1016/j.jbc.2026.113103

Stephanie Holley*,‡, Gary Asmussen‡, Becky Lam, Zhonglin Zhao, Brian Freed, Lilu Guo, Zuzana Dostalova, Buyun Tang, Michael Kothe, Paul Lang, Donghui Wang, Martin Hanus, Alexei Belenky, Mandy Cromwell, Alla Kloss, and Tatiana Gladysheva*

From the Research and Development, Sanofi, Cambridge, Massachusetts, USA

Reviewed by members of the JBC Editorial Board. Edited by George M. Carman

Adrenoleukodystrophy (ALD or X-ALD) is a rare devastating neurological disease caused by mutations in the *ATP binding cassette D1 (ABCD1)* gene, the product of which is involved in the transport of very long-chain fatty acids (VLCFAs) into peroxisomes for degradation by β-oxidation. Deficiency in ABCD1 results in VLCFAs accumulation in many tissues, including the brain and spinal cord. Elevated VLCFA levels, specifically C26:0, are consistent biochemical markers of ALD and are implicated in the ALD pathogenesis. ALD disease is manifested by multiple phenotypes: the most severe cerebral disease (cerebral ALD, cALD), adrenomyeloneuropathy (AMN) and adrenal insufficiency (Addison disease). VLCFA accumulation is a hallmark of all ALD phenotypes, and reduction/normalization of VLCFA levels is an attractive approach for the treatment of all ALD manifestations. VLCFAs synthesis involves enzymes from elongase of very long-chain fatty acids (ELOVL) enzyme family with ELOVL1 being a rate-limiting enzyme in C26:0 synthesis, making ELOVL1 an attractive target for medical intervention in ALD *via* Substrate Reduction Therapy (SRT). In this paper, we describe the *in vitro* assays established to support medicinal chemistry efforts to develop small-molecule ELOVL1 inhibitors for ALD. Notably, we developed novel, breakthrough *in vitro* methods to monitor enzymatic and cellular ELOVL1 activity, enabling high-throughput screening (HTS) of Sanofi library collections. We successfully identified CNS-active, small-molecule ELOVL1 inhibitors shown to be efficacious in the reduction of C26:0 VLCFA levels in cells and multiple tissues, including brain and spinal cord, in animal models.

Adrenoleukodystrophy (ALD) is a rare neuromuscular heterogeneous genetic disease that mainly affects the nervous system and the adrenal gland and is caused by mutations in the *ABCD1* gene (1). ALD presents with multiple manifestations. In men, these include cerebral ALD (cALD), the most aggressive brain inflammation and demyelination with short life expectancy (2–4 years after disease onset); Adrenomyeloneuropathy (AMN), a slow-progressing spinal cord degeneration; and adrenal insufficiency (Addison's disease). About 35 to 40% of boys with ALD will develop cerebral form of the disease in childhood, and 20% of adult men with AMN will develop cALD later in life; about 80% of male patients develop Addison's disease during the course of ALD. The most common adult phenotype of ALD is AMN, with onset later in life (between the ages of 20 and 40 in male patients) (2, 3).

Heterozygous female patients also develop the disease, predominantly suffering from slow-progressing AMN with onset later in life (between ages 40 and 50), and extremely rarely present with other ALD manifestations (4–6).

Hematopoietic stem cell transplantation was a first-line treatment for Childhood Cerebral ALD (CCALD); this has been shown to halt cerebral disease progression if performed at an early stage of the disease (7–9). Recently developed lentiviral gene therapy promises an immense potential in ALD treatment but is currently approved for CCALD only and has limited understanding of the long-term safety of this treatment, with reported hematologic malignancies in a subset of patients receiving this treatment (10, 11). AMN for men and women is still a major clinical form of the disease without any approved or marketed treatment, and represents a high unmet medical need.

ALD is genetically caused by mutations in the *ABCD1* gene, which encodes for the Adrenoleukodystrophy Protein (ALDP) responsible for the transport of VLCFA to peroxisomes for degradation (12–14). Multiple mutations described in the *ABCD1* gene are manifested in various deficits in the transporter, resulting in the accumulation of VLCFA in multiple organs, including spinal cord and brain of patients with ALD. Specifically, accumulated C24:0 and C26:0 fatty acids are thought to be responsible for ALD manifestations and pathology (15, 16).

There are 7 ELOVL enzymes described in humans with various substrate specificities towards VLCFAs. ELOVL1 enzymatic activity is a rate-limiting step in *de novo* synthesis of VLCFAs C24:0 and C26:0 (17, 18). Modulation/inhibition

‡ These authors contributed equally to this work.
* For correspondence: Stephanie Holley, Stephanie.Holley@sanofi.com; Tatiana Gladysheva, Tatiana.Gladysheva@sanofi.com.

of ELOVL1 activity has the potential to decrease and normalize VLCFA levels in all patients with ALD; and might serve as a substrate reduction therapy approach shown to be successful in the clinic for rare diseases where enzyme replacement therapy limitations hamper better treatment outcomes. The first SRT treatments approved for Gaucher disease (19–21) validated the SRT approach and paved the way for several currently active clinical trials for other rare diseases (Fabry (22), Niemann-Pick type-C (23) and Pompe disease (24)).

Here, we describe the initial steps of a small-molecule drug discovery program aiming to identify and develop small-molecule ELOVL1 inhibitors as substrate reduction therapy for ALD treatment.

Along the course of our journey, we developed a robust *in vitro* platform using multidisciplinary methods and technologies, including comprehensive set of biochemical and cell-based assays with different throughput capabilities, lipidomics and Gas Chromatography-Mass Spectrometry (GCMS) compounds profiling and structural biology tools to inform the medicinal chemistry team on compounds' potency, Mechanism of Action (MoA), selectivity, *etc.* This approach enabled in-depth Structure Activity Relationship (SAR) understanding and development of a potent, selective, CNS penetrant ELOVL1 inhibitor showing significant reduction of C26:0 VLCFA in the cells and multiple tissues, including brain and spinal cord, in animal models (recently published) (25).

(Note: chemical structures of ELOVL1 inhibitors are not disclosed).

Results

Two-pronged approach to identify ELOVL1 hits through screening efforts

To augment the hit finding campaign, we set up a two-pronged approach and screened Sanofi's small-molecule library collections in biochemical and in cell-based phenotypic HTS formats. Thus, we have identified ELOVL1 inhibitors that suppressed VLCFAs synthesis in a biochemical assay and in cells. Overall, about 724,000 compounds were screened by this effort.

In a biochemical HTS 406,000 small molecules from Sanofi library collections were screened, resulting in a low hit rate of 0.1% average (ranging from 0.03 to 0.4% depending on the collection screened); few promising chemical series were identified in this campaign (data not shown).

In the phenotypic HTS, about 485,000 small molecules from Sanofi library collections were screened with an average hit rate of 2.3%. This screen was performed as a complementary approach to biochemical HTS to expand hit finding. Hits from the phenotypic HTS lacking ELOVL1 potency were not followed up. One new chemical series with ELOVL1 activity was identified from this screen and followed up. Overall, the 20-fold higher hit rate in the phenotypic screen demonstrates the value of a dual-screening strategy, as the cell-based approach captured chemotypes that were missed by the biochemical assay alone, substantially expanding the chemical space for hit finding.

Biochemical assays to monitor activity and specificity of ELOVL1 small-molecule inhibitors

Novel high-throughput method for VLCFA detection

To identify ELOVL1 small-molecule inhibitors, we developed a novel biochemical assay using ELOVL1 protein in microsomal preparation to monitor its enzymatic conversion of C22-Coenzyme A (C22-CoA) to C24-Coenzyme A (C24-CoA) utilizing a stable isotope-labeled deuterated C22-CoA substrate to enhance sensitivity. Detection was carried out using a RapidFire system hyphenated with a triple quadrupole MS/MS instrument. This method includes several breakthrough steps developed in our lab for hydrolysis and fatty acids extraction as well as for MS/MS read-out; it enabled reaction miniaturization in 384-well format to perform MTS/HTS and follow-up studies.

In contrast with traditional low-throughput hydrolysis and extraction methods used in thin-layer chromatography (TLC)-based lipid analysis, or conventional LC-MS analysis, the optimized workflow developed for the ELOVL1 RapidFire-MS/MS assay was specifically designed for miniaturization, speed, and reproducibility. In the optimized method, hydrolysis was performed in-plate by directly adding 7.5 N potassium hydroxide (KOH) to the 384-well reaction plates, sealing, and incubating at 80 °C for 3 h. This approach efficiently liberates fatty acyl moieties from CoA thioesters while eliminating the need for sample transfer and neutralization steps required in conventional workflows. Following hydrolysis, fatty acids were extracted by the addition of acetonitrile and brief centrifugation, and the clarified supernatant was directly injected into the Rapid Fire-MS/MS system without solvent evaporation or reconstitution. During method development, hydrolysis and extraction efficiency were rigorously monitored by varying reagent concentrations, incubation times, and temperatures, with iterative adjustments bringing the fatty acid recovery rate close to 100% in the final protocol.

Traditional TLC workflows, which have historically been favored for their simplicity, visual band separation, and low instrumentation requirements, typically involve hydrolysis in glass tubes using strong acid or base in large-volume organic solvents. These workflows often require overnight incubation and multiple manual transfer steps, including neutralization and solvent evaporation. Fatty acid extraction generally requires repeated extractions with chloroform, methanol, or hexane, followed by drying and resuspension prior to analysis. While conventional methods remain valuable for low-throughput lipid profiling or quantitation, they are labor-intensive and not suited for screening applications. By contrast, the optimized RapidFire-MS/MS-compatible method enables the parallel processing of 6 to 8 384-well plates per day, significant reduction of sample loss and

variability while delivering the robust, quantitative analysis required for medium- to high-throughput screening campaigns.

ELOVL1 microsomal enzyme activity assay

To establish optimal assay conditions and determine Michaelis–Menten kinetics, we first titrated the enzyme and measured product formation over time to define linear reaction parameters (Fig. 1*A*). Based on these findings, ELOVL1 concentration of 250 μg/mL and a reaction time of 150 min were selected for the subsequent experiment. Once time and enzyme concentration dependencies were established, we titrated the substrate acceptor (C22-CoA), donor (malonyl-CoA), and cofactor (NADPH) to determine their half-maximal concentrations, the Michaelis constants (K_m) (Fig. 1*B*, 61 μM C22-CoA, 0.9 μM Malonyl-CoA, and 2.5 μM NADPH). Next, we set substrate and cofactor concentrations at their half-maximal values and re-titrated the enzyme to establish the reaction balanced conditions (Fig. 1*C*) which enables identification of inhibitors acting through competitive, uncompetitive, or non-competitive mechanisms. We utilized the reaction product, Coenzyme A (CoA), along with other CoA derivatives (Fig. 1*D*), to establish a positive control inhibitor for future experiments.

Finally, under balanced conditions (75 μg/mL ELOVL1, 10 μM C22-CoA, 0.9 μM Malonyl-CoA, and 250 μM NADPH), we validated the assay's robustness (Fig. 1*E*) and reproducibility to screen for ELOVL1 inhibitors by conducting a signal uniformity plate test. Using DMSO as a 0% inhibitor control (max signal), we tested the inhibitor at its IC_{50} concentration (50% inhibition, mid signal) and at full inhibition (100% inhibition, min signal), to demonstrate robustness, precision, and reproducibility of the assay within a single plate and across multiple plates in independent experiments performed in three consecutive days (data shown for 2 days). The assay achieved a Z′ factor greater than 0.5, confirming its robustness and suitability for high-throughput screening.

The initial biochemical MTS was performed at a final compound concentration of 10 μM. The confirmed hit rate in the first collection of 36,000 compound screens was relatively low: 0.07% with a cut-off at 30% inhibition (>3 × SD); in the second screen of 38,000 compounds the confirmed hit rate was 0.03%. In subsequent evaluations of the libraries, the screening compounds concentration was increased to 30 μM to enhance the recovery of chemical matter, leading to a higher hit rate of 0.1% with a cut-off at 30% inhibition (>3 × SD). Hit confirmation was performed using fresh compound stocks, with the hit confirmation rate being on average 75% for compounds that showed inhibition greater than 50% in MTS. Confirmed hits were then subjected to purity assessment and medicinal chemistry evaluation for potential lead finding. Extensive back screening was performed to follow up on initial HTS hits which confirmed identified hits and established limited SAR. An active medicinal chemistry effort was initiated at this point when promising scaffolds for ELOVL1 inhibitors were identified from HTS and back screening campaigns. The low

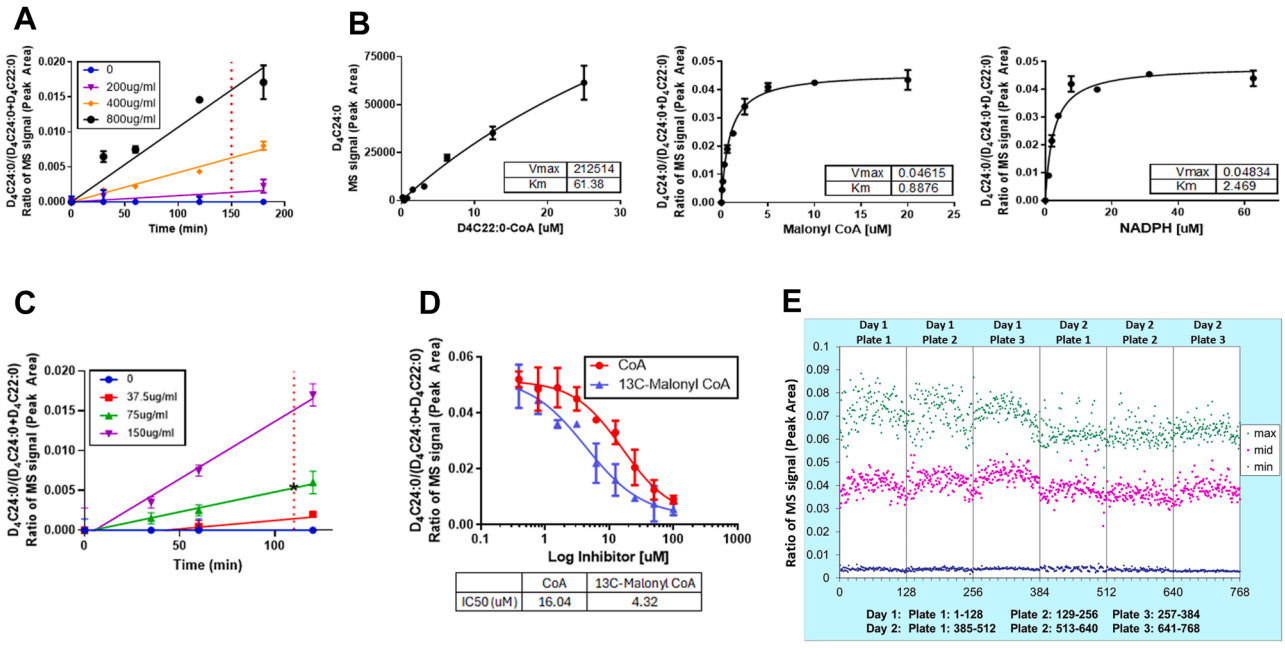

Figure 1. ELOVL1 enzyme activity assay development and validation. *A*, ELOVL1 microsomes activity was tested at different enzyme concentrations and saturated substrate concentrations (200 μM d4C22:0-CoA, 20 μM Malonyl-CoA, 1 mM NADPH) to establish linear reaction conditions. *B*, using 250 μg/mL ELOVL1 at 150-min reaction time, the *Km* values of d4C22:0-CoA, Malonyl-CoA and NADPH were determined as 61 μM, 0.9 μM, and 2 μM, respectively. *C*, ELOVL1 microsomes activity was tested at balanced reaction condition (10 μM d4C20:0-CoA, 0.9 μM Malonyl-CoA, 250 μM NADPH) and different enzyme concentrations to establish final assay parameters noted by the *red dotted line* and *asterisk*. *D*, inhibition of ELOVL1 activity by CoAs; IC_{50}s were determined. *E*, representative six 384-well plate data for the assay signal uniformity test assessing the consistency of high-medium-low (HML) enzyme activity across one and multiple 384-well plates; assay was performed on three different days, the data shown for 2 experimental days, Z′ ranged from 0.55 to 0.77.

biochemical hit rates underscore the isoform selectivity of the assay and the challenging nature of the ELOVL1 target. The high confirmation rate validates the assay's reliability for identifying genuine inhibitors and supports its use as the primary biochemical screening platform.

Additional elongase microsomal enzyme activity assays

To evaluate compound selectivity across the elongase family, we measured compound potency against additional elongases beyond ELOVL1. All assays were developed analogously to the ELOVL1 assay using microsomes from SF9 cells overexpressing each enzyme, with linear reaction conditions and Km values established for each isoform (Figs.S1–S4); CoA served as a reference inhibitor across assays. Using microsomal assays for ELOVL3 (Fig. S1, *A–D*), ELOVL6 (Fig. S2, *A–D*), and ELOVL7 (Fig. S3, *A–E*), we observed clear differences in compound activity across family members, enabling assessment of isoform selectivity. The corresponding IC_{50} values are presented in Table 2 and the respective assay conditions are summarized in Table 3. Consistent with their known functional overlap, ELOVL3 and ELOVL7 displayed elongation profiles that partially overlapped with ELOVL1, whereas ELOVL6 showed a distinct activity pattern reflecting its upstream role in the pathway (Fig. S9). Structural modeling based on the available ELOVL7 crystal structure further supported differential compound binding interactions among elongase isoforms (data not shown).

We also developed a zebrafish ELOVL1b microsomal assay (Fig. 4, *A–E*), determined balanced conditions (304.9 μM C22-CoA, 1.4 μM Malonyl CoA, and 2.6 μM NADPH) and assessed compound potency and selectivity. The zebrafish enzyme assay showed a potency trend for the compounds consistent with the human assay, reinforcing cross-species target engagement. To study other species selectivity of ELOVL1 inhibitors, we developed species-specific cell-based assays described below.

Purified ELOVL1 enzyme activity assay

All elongase assays described above utilize microsomal enzymes to monitor activity. To understand the relationship between microsomal and purified enzyme activities, we developed an ELOVL1 enzyme activity assay using purified ELOVL1 enzyme. ELOVL1 was purified from Sf9 insect cells as a C-terminal fusion with enhanced GFP. Due to the low yield of purified ELOVL1, only a limited number of experiments were performed using this enzyme. Initial purified ELOVL1 enzyme activity was low. To mimic physiological conditions, ELOVL1 was embedded in proteoliposomes, which allowed for a significant increase in enzyme activity. Purified ELOVL1 alone produces three-keto-C24 and CoA. An assay was developed to monitor the enzymatic conversion of C22-CoA to three-keto-C24-CoA.

First, for assay development, the detection of specific production of three-keto-d4 C24-CoA was determined in a matrix experiment. As shown in Figure 2*A*, three-keto-d4 C24-CoA is only produced in the presence of purified ELOVL1 enzyme, malonyl CoA and d4C22, confirming the intrinsic activity of ELOVL1 enzyme. Once specific activity was confirmed, the enzyme titration experiment was performed, where product formation was measured over time to identify linear reaction parameters (Fig. 2*B*). Using the established enzyme concentration and time dependencies (8 μg/mL and 120 min reaction), we titrated the substrate donor (Malonyl-CoA) and acceptor (C22-CoA) to determine their half maximal concentrations (Fig. 2*C*, 10 μM d4C22, 4.5 μM Malonyl-CoA). Next, we set substrate concentrations at their half-maximum values and re-titrated the enzyme (Fig. 2*D*) to establish balanced reaction conditions (8 μg/mL proteoliposome, 10 μM d4C22, 5 μM Malonyl-CoA), which enables us to study ELOVL1 inhibitors potency and compare to potency values obtained in the microsomal enzyme activity assay. The purified ELOVL1 enzyme assay described here produced IC_{50} values within three-fold of the ELOVL1 microsomal assay (Fig. 2, *E* and *F*), validating the routine use of the ELOVL1 microsomal assay for compound potency screening in support of medicinal chemistry efforts, SAR understanding and compound development.

Identification of abundant and ELOVL1-responsive lipids through cellular lipidomics profiling

Measurement of VLCFAs in cells is proven to be challenging due to most VLCFAs being incorporated in lipids as

Table1
Summary of lipidomics profiling data for human fibroblasts

Lipid class	Number of lipids	Chain length	Max fold change	Phenotypes and relative abundance of the lipid
LPC	6	C26–C30	8–99.5	CCALD ≈ AMN > Healthy
PC	8	>C24	3–(>100)	CCALD ≈ AMN > Healthy
SM	1	C26	>3	CCALD ≈ AMN > Healthy
Free FA	10	C26–C30	4–8	CCALD > AMN > Healthy
HexCer	1	C26	>3	CCALD ≈ AMN > Healthy
Oxidative	6	Isoprostanes, Oxidated FFAs	Up to >10	CCALD ≈ AMN > Healthy
Carnitines	15	C14-C22	3-(>100)	CCALD > AMN ≈ Healthy
DG	3	Short chain	2.5–4	AMN > CCALD ≈ Healthy
TG	15	Very Long Chain	3–(>100)	CCALD > AMN > Healthy
Cer	2	C26	>3	CCALD ≈ AMN > Healthy
LacCer	1	C26	>3	CCALD ≈ AMN > Healthy
O-acyl Cer	2	C16	7–8	CCALD > AMN > Healthy
PE	4	Long Chain, poly-unsat	4–6	CCALD ≈ AMN > Healthy
PG	4	Short Chain (sat and poly-unsat)	>3	AMN > Healthy
PI	4	Long Chain, poly-unsat	4–5	AMN > Healthy
LPI	1	C20:4	>12	Healthy > CCALD ≈ AMN

SMC26:0 was chosen as biomarker to monitor ELOVL1-driven cell-based activity.

Table 2
IC_{50} values determined for ELOVL enzymes

Compound	ELOVL1 IC_{50} (μM)	ELOVL3 IC_{50} (μM)	ELOVL6 IC_{50} (μM)	ELOVL7 IC_{50} (μM)
Compound A	0.044	>99.01	>99.01	>99.01
Compound B	0.072	>99.01	>99.01	>99.01
Compound C	0.027	88.228	ND	>99.01
Compound D	0.141	>99.01	>99.00	ND
Compound E	0.02	>99.01	ND	ND
Compound F	0.011	>99.01	>99.01	ND
Compound G	0.054	>99.01	ND	>99.01
Compound H	0.261	>99.01	ND	>99.01
Compound I	0.106	>99.01	ND	>99.01
Compound J	0.039	77.776	ND	>99.01
Compound K	0.023	ND	>99.01	ND

ND, not determined.

well as analytical sensitivity limitations, further complicated by sample complexity, resulting in substantial matrix effects. Consequently, direct analysis of VLCFAs is not suitable for high-throughput cell-based assays, which could support medicinal chemistry efforts in drug discovery and development. To overcome these challenges, we developed cell-based assays to monitor the production of a series of lipids with VLCFAs, whose levels correlate with ELOVL1 levels and activity in the cell. To enable such assay development, we have profiled fatty acids and lipids in fibroblasts from healthy controls, patients with CCALD, and patients with AMN for assessment of relative lipids abundance by type, extent of accumulation of VLCFAs in different types of lipids, and different phenotypes to select cell line for the assay with highest level of C26:0 and the most suited lipids species to ensure broad linear dynamic range of the assay.

For the selection of the cell line with higher C26:0 levels, data for total FAs were compared from all available cell lines. The total FA profiling in human fibroblasts was carried out by GC-MS analysis of the samples after hydrolysis, converting FAs incorporated in lipids into free FAs. The summary is shown in Figure S8. Samples showed correlation of VLCFAs levels with the phenotype severity but displayed differences in total FA levels and VLCFAs specifically. That underscored the utility of the data normalization that enabled selection of the cell line for the assay development.

A lipidomics platform established in-house was then applied to identify lipid classes containing C26:0 chains which are most suited for development of the lipid-based screen. The following key selection criteria were applied for choosing the lipid species that can be used for the assay: sensitivity to the phenotype, clear trending with severity, big fold change compared with controls and good *p*-values (to ensure a good dynamic range), significant abundance, free of interferences in a high-throughput RapidFire MS/MS screen (where, in absence of chromatographic separation, sample cleanup is limited to desalting). The lipids of choice were further validated with ELOVL1 knockdown (KD) experiments. Figure 3 shows the results of global lipid profiling of human fibroblasts normalized by total lipids measured by our method. The data is presented separately for positive and negative mode of detection in mass spectrometer (Fig. 3*A*). Since quantitation of thousands of lipids in one LC-MS method is not possible and not necessary in this case, global profiling was optimized as semi-quantitative method focused on best possible coverage of the lipidome. Figure 3*A* shows a total composition, where signals of all lipids are summarized by lipid type (giving a total relative abundance of each type of lipid, where species of the same lipid type with different side chains are all added together). As shown in the figure, total lipid composition is not affected by disease or the phenotype, while we have seen elevated levels of individual lipids containing VLCFAs in samples from X-ALD patients (Fig. 3*B* and Table 1). Figure 3*B* shows several lipid types that are most abundant in human fibroblasts, including PC, SM, Pes, o-Pes and PIs. We have identified lipid species which show the most significant fold change compared to control and summarized the findings in Table 1 by lipid types, side chains and the phenotype. It is interesting that while lipid species incorporating VLCFAs are trending with severity of the phenotype, being most elevated in CCALD fibroblasts, intermediate in AMN and lowest in control cells, few species are close in both phenotypes and higher than in controls. Few lipid types with short, long and poly-unsaturated side chains are higher in AMN cells than in CCALD and LPI C20:4 is up to 12-fold higher in control fibroblasts than in CCALD and AMN cells (Table 1). These change patterns, if further explored, may yield a promising method for early identification of the phenotype and potential for disease progression into CCALD. To choose the relevant, highly abundant, and sensitive lipids

Table 3
Biochemical assay conditions used for different ELOVL enzymes

Condition	ELOVL1	ELOVL3	ELOVL6	ELOVL7	zebrafish ELOVL1
Enzyme [μg/ml]	75	30	20	30	75
Fatty acyl-CoA [μM]	10	7.5	5	7.5	10
Malonyl-CoA [μM]	0.9	2.5	5	1	1
NADPH [μM]	250	250	300	250	250

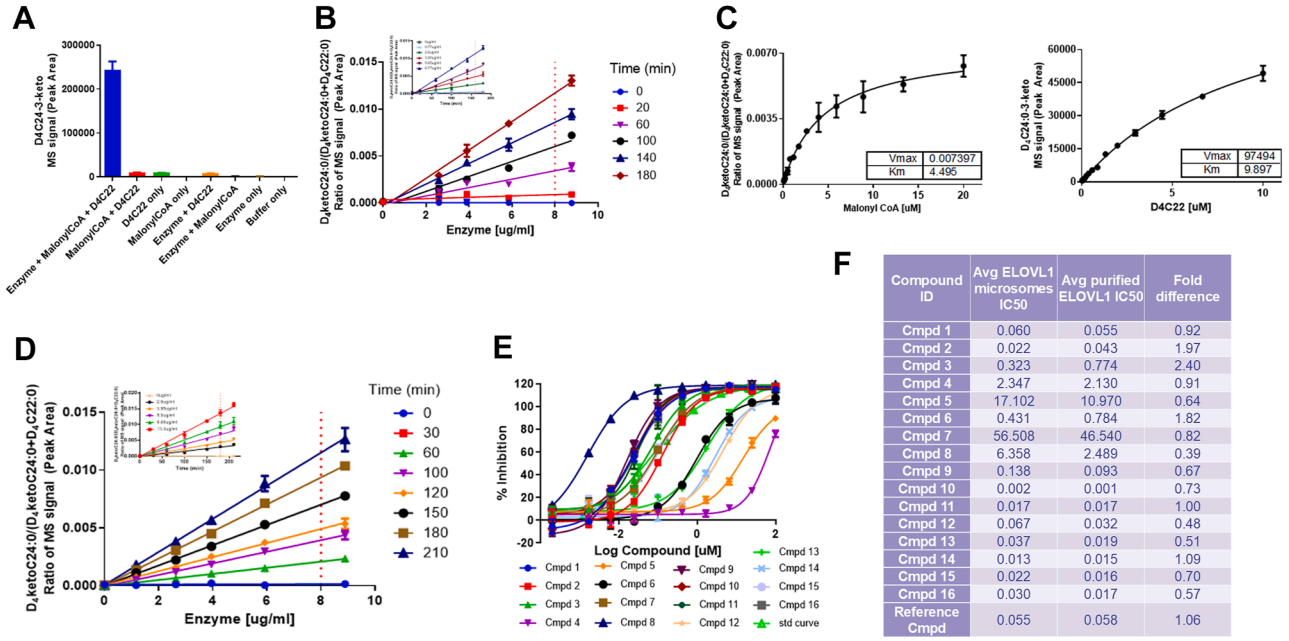

Compound ID	Avg ELOVL1 microsomes IC50	Avg purified ELOVL1 IC50	Fold difference
Cmpd 1	0.060	0.055	0.92
Cmpd 2	0.022	0.043	1.97
Cmpd 3	0.323	0.774	2.40
Cmpd 4	2.347	2.130	0.91
Cmpd 5	17.102	10.970	0.64
Cmpd 6	0.431	0.784	1.82
Cmpd 7	56.508	46.540	0.82
Cmpd 8	6.358	2.489	0.39
Cmpd 9	0.138	0.093	0.67
Cmpd 10	0.002	0.001	0.73
Cmpd 11	0.017	0.017	1.00
Cmpd 12	0.067	0.032	0.48
Cmpd 13	0.037	0.019	0.51
Cmpd 14	0.013	0.015	1.09
Cmpd 15	0.022	0.016	0.70
Cmpd 16	0.030	0.017	0.57
Reference Cmpd	0.055	0.058	1.06

Figure 2. Purified ELOVL1 enzyme activity assay development and validation. *A*, purified ELOVL1 activity required the presence of both substrates. *B*, purified ELOVL1 protein activity was tested at different enzyme concentrations using saturated substrate concentrations to establish reaction linearity. *C*, using 8 μL/mL purified ELOVL1 enzyme at 160-min reaction time, the Km values of d4C22:0-CoA, and Malonyl-CoA were determined as 9.8 μM and 4.5 μM respectively. *D*, purified ELOVL1 enzyme was re-titrated at balanced conditions to establish final reaction parameters. *E*, 16 compounds were tested in a dose–response manner using purified ELOVL1. *F*, IC_{50}s determined with the purified ELOVL1 enzyme are in good agreement with IC_{50}s determined in the microsomal ELOVL1 assay.

whose levels change following the ELOVL1 enzyme activity in cells, we have selected those species which showed elevated level in disease (trending with the phenotype severity and showing biggest fold change). Lipidomic profiling of fibroblasts from X-ALD patients yielded several robust lipid biomarkers that reflect alterations in VLCFAs levels with high sensitivity (Fig. 3*B* and Table 1). Among these, C26-containing lipids—C26 lysophosphatidylcholine (LysoPC C26:0 and C26:1), C26 sphingomyelin (SM), C26 Ceramide, C26 triglyceride (TG) and C26 phosphatidylcholine (PC). Notably, C26:0 LysoPC and C26:0 PC exhibited the highest fold changes, most significant *p*-value. But LysoPC has relatively low abundance in fibroblasts and sensitive to sample stability because it can be formed as a result of hydrolysis of PC under freeze-thaw conditions and exposure to temperatures above −80 °C, which would introduce additional variability in HT assay. PC C26:0 and SM C26:0 had the highest abundance in CCALD fibroblasts compared to controls.

To further study the role of ELOVL1, we performed knockdown experiments to examine its function in CCALD

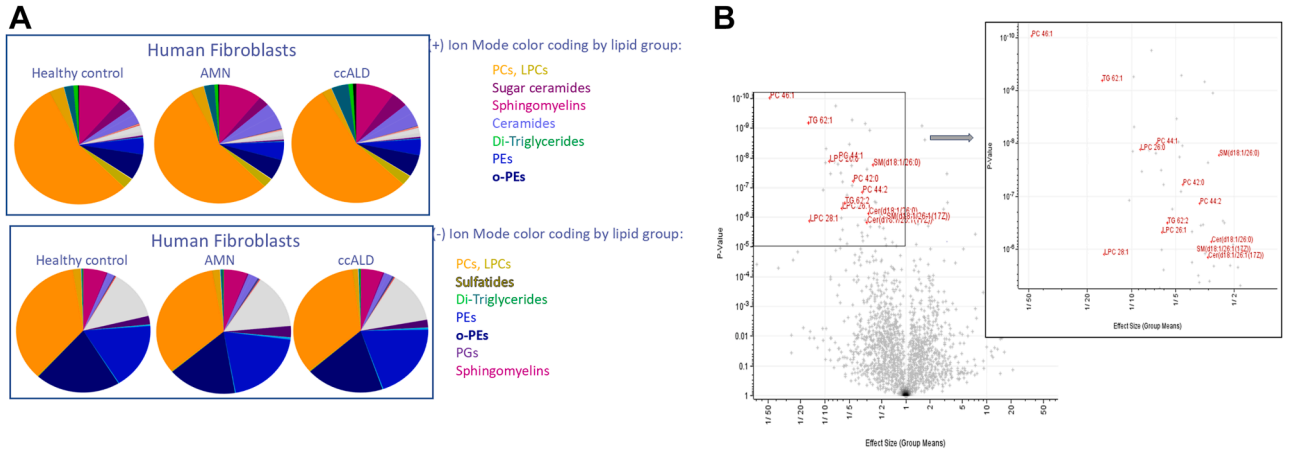

Figure 3. Global lipidomic profiling of CALD, AMN, and matched Healthy patient's fibroblasts. *A*, relative total abundance of lipids (summarized by lipid types and normalized by total measured lipids) showing a conserved overall lipid composition of human fibroblasts in all three phenotypes. The data summarized separately for lipids detected in the positive (*top*) and the negative (*bottom*) MS detection mode. *B*. Volcano plot. Among the significantly altered lipids, C26:0 lysophosphatidylcholine (LysoPC) and C26:0 sphingomyelin (SM) emerged as the most reliable disease and target biomarkers, based on their fold change, statistical significance (*p*-value), and relative abundance in patients' fibroblasts.

patient fibroblasts (Fig. 4*A*). SM C26:0 is abundant in CCALD patient cells; however, its level is significantly decreased upon *ELOVL1* knockdown by siRNA, as shown by the ratio of SM C26:0 to SM C22:0 normalized to the internal standard C17 (Fig. 4*B*). Worthy to notice is that ELOVL1 knockdown caused a significant decrease of SM C26:0 level (Fig. 4*C*) but not SM C22:0 level (Fig. 4*D*).

Our data suggest that ELOVL1 knockdown *via* siRNA in CCALD cells resulted in the most pronounced reduction in several VLCFAs containing lipids, with C26:0 PC and SM levels showing the best combination of relative abundance and fold change (Table 1, Figs. 4*A* and 5*B* (SM shown only)). Initially both markers were evaluated as candidates for MTS/HTS assay, but PC (18:1/26:0) in the absence of front end chromatographic separation was suffering from interferences, while SM(18:1/26:0) did not have this issue and was passing all the other selection criteria. These findings establish SM C26:0 as a robust, ELOVL1-responsive biomarker suitable for high-throughput screening.

Cell-based assays to support small-molecule ELOVL1 inhibitor identification and development

The robust cell-based assays using human CCALD or AMN patients' fibroblasts were developed to monitor selected lipids mentioned above; the most robust signal used for ELOVL1 activity assessment in the CCALD cells was attributed to C26:0 SM (SM18:1/26:0) where a variety of different cell numbers per well were tested at different time points and were used to identify the signal window for the phenotypic cell-based screening (Fig. 5*A*); RapidFire MS/MS method was used to monitor the signal of different lipids (SM, PC, Lyso PC) (Fig. 5*B*). A cell viability assessment with 250 to 2000 cells per well from 24 to 72 h was used to develop a complementary human cell toxicity assay (Fig. 5*C*). Complementary to biochemical ELOVL1 activity HTS we also performed a phenotypic HTS using patients CCALD fibroblasts; and screened about 485,000 compounds from Sanofi library collections at 10 μM final concentration to identify small molecules inhibiting the VLCFA pathway. An in-house medium throughput screening was performed with over 110,000 compounds from various Sanofi collections followed up with hit confirmation (Fig. 6*B*) and then with dose response in lipid lowering and cell viability assays (Fig. 6*C*) using CCALD patient fibroblasts. Hit rates varied between collections from 0.72 to 4.8% with Z′ values between 0.56 and 0.83. (Fig. 6*A* representative run. Additional external screening was performed with a total of 375K compounds screened at 10 μM, followed up with hits confirmation and dose response assays (data not shown). Toxic compounds were eliminated by testing hits in a cell viability assay using the CCALD fibroblasts; cell viability assay development is shown in Figure S5. Briefly: first, cell confluence was assessed with different numbers of cells per well and at various time points (Fig. S5*A*), then the assay window was established by monitoring cell growth at different time points in the absence or presence of reference inhibitor, epoxomicin. As shown in Figure S5*B*, the final assay conditions were selected as 750 cells/well (in 384-well plates) at the 72-h time point.

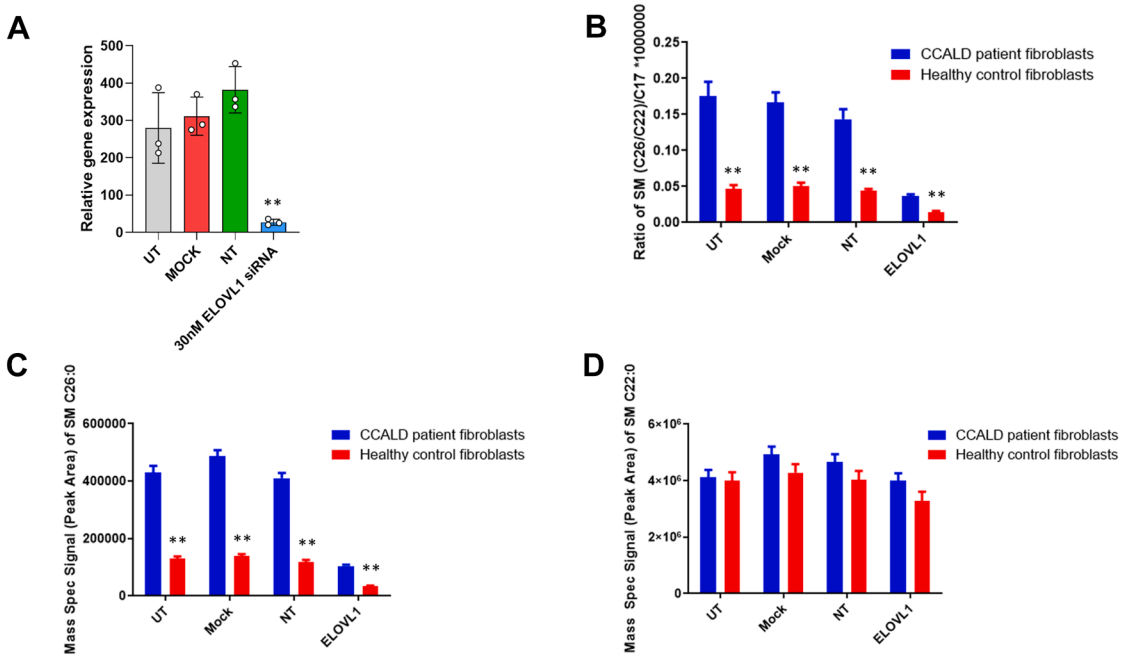

Figure 4. ELOVL1 knockdown in CCALD human patient fibroblasts. *A*, siRNA-mediated *ELOVL1* knockdown was performed in CCALD disease fibroblasts using 30 nM targeting siRNA. UT = untreated; Mock = control for transfection process (no siRNA); NT = non-targeting siRNA. *B*, cell-based assay biomarkers: SM C26:0 is abundant in CCALD patient cells; and its level is significantly decreased upon *ELOVL1* knockdown by siRNA. Ratio of SM C26:0 to SM C22:0 was normalized using internal control C17. *C*, peak area of mass spectrometry signal for SM C26:0. *D*, Peak area of mass spectrometry signal for SM C22:0.

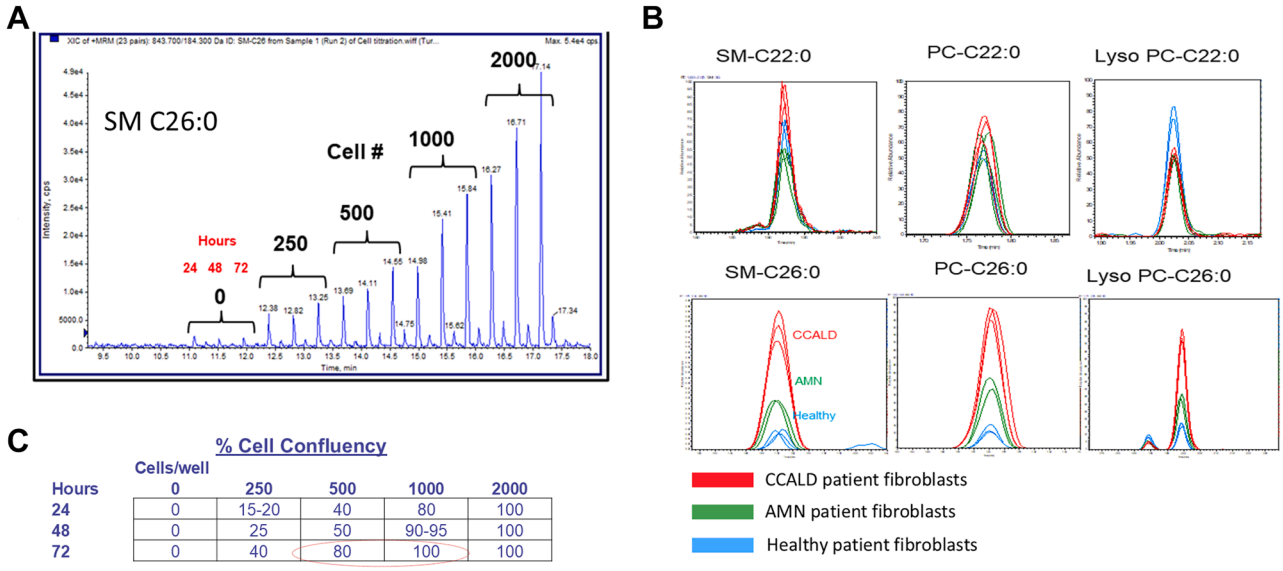

C

% Cell Confluency

Hours \ Cells/well	0	250	500	1000	2000
24	0	15-20	40	80	100
48	0	25	50	90-95	100
72	0	40	80	100	100

Figure 5. Cell-based assay to assess ELOVL1 inhibitor potency. RapidFire/MS-MS method was used for MTS cell-based assay to monitor C26:0 SM signal. *A*, a titration of cell number at 0, 24, 48 and 72 h; SM C26:0 signal was recorded by Rapidfire. *B*, SM, PC, and lysoPC C22:0 and C26:0 show different sensitivity for the disease state. VLCFAs in sphingolipids and phospholipids: SM C26:0; PC C26:0 and LysoPC C26:0 are elevated in X-ALD fibroblasts, both in AMN and CCALD, compared to control fibroblasts. *C*, CCALD cell confluency percentage was monitored at different cell concentrations over time; 750 cells/well and 72-h growth timepoint were chosen as final assay conditions.

Epoxomicin potency, IC_{50}, was also determined as 0.02 μM (Fig. S5*C*), which is in good agreement with the literature data published for several cell lines.

Orthogonal cell-based assays were developed to assess compound potency in multiple species, including mouse (Fig. S7*A*), rat, dog (data not shown) and minipig cells (Fig. S7*D*).

Most compounds show IC_{50} within a three-fold difference between human and mouse assays (Fig. S7*C*). Complementary cell viability assays were developed in all above-mentioned species to assess the compound effect on cell viability (data not shown). All orthogonal assays including cell viability assays were developed similarly to human assays (Fig. S7, *A* and *B* – examples of several steps in the assay development). The

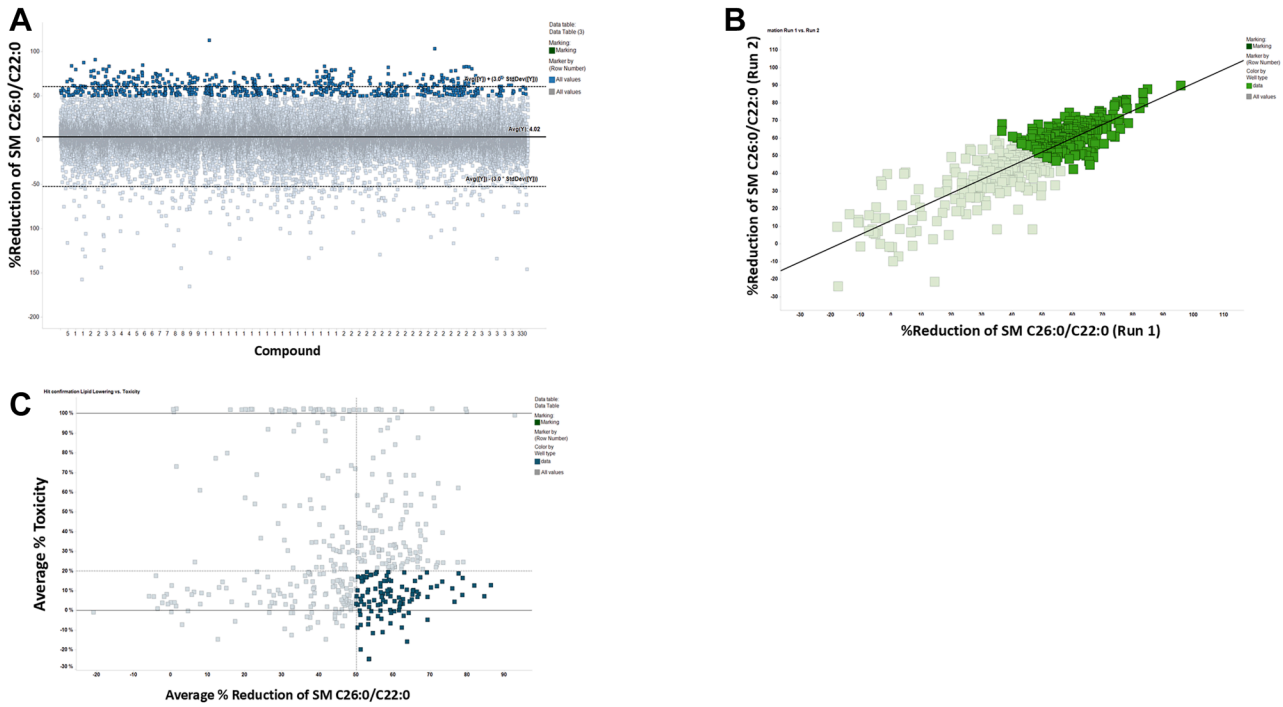

Figure 6. Cell-based MTS monitoring SM C26:0 marker Summary. *A*, About 36,000 compounds screened from SASC core 1 Sanofi library at 10 μM (final concentration) using CCALD fibroblasts; 675 hits (>50% reduction at 10 μM) were identified yielding a 1.9% hit rate. *B*, hit confirmation rate was 51% for compounds with >50% reduction of SM C26:0 normalized to SM C22:0. *C*, confirmed hits were tested in a cell viability assay to eliminate toxic compounds; 106 compounds had >50% reduction of SM C26:0 normalized to SM C22:0 and < 20% toxicity at 10 μM.

robust Z′ values and consistent cross-species potency demonstrate that this cell-based platform is suitable for supporting medicinal chemistry optimization effort and predicting *in vivo* efficacy across preclinical species.

Assessing the mechanism of action (MoA) of ELOVL1 inhibitors by mapping the elongase pathway changes

Since our screening assays are based on measurement of lipids containing C 26:0 side chain, we have developed a gas chromatography mass spectrometry (GC-MS) method to monitor multiple Fatty Acids and studied their level changes upon ELOVL1 inhibitors treatment (Figs. 6, *A* and *B* and 7). It allowed us to gain a better understanding of the MoA of active compounds identified in our screens and to confirm that the reduced levels of VLCFAs-containing lipids in cells resulted from selective inhibition of ELOVL1 and not by modulating lipid synthesis. Our GC-MS assay allowed for monitoring 34 fatty acids quantitatively with chain lengths ranging from C11:0 to C26:0, including 14 saturated, 8 mono- and 12 polyunsaturated fatty acids (as described in the earlier publication) (25). We were able to monitor changes in elongation, oxidation, and desaturation of VLCFA using unlabeled and stable isotope-labeled fatty acids (including 13C18-C18:0; 13C6-C22:0; 13C6-C26:0, *etc.*). Using this approach, we have characterized selected compounds for their MoA (Fig. 7).

For the implementation of a comprehensive approach to data analysis, we created hit maps, allowing for simple and robust visualization of the compounds' effect. Based on these maps, the inhibitory effect of selected compounds was compared to the effect of the ELOVL1 knockdown in cells (Fig. 7). To make this analysis more robust, we compared the compound effect to the effect of knockdown of a few other critical players in the ELOVL1 elongase cascade, including ELOVL6 and Ceramide synthase 2 (CerS2) (Fig. 8). Two ELOVL1 inhibitors presented on this graph show the significant changes in many lipids' levels, including SM, PC, LysoPC and Ceramide families in a manner that mirrored ELOVL1 KD effect, and not ELOVL6 KD or CerS2 KD effects in CCALD fibroblasts (Fig. 8). ELOVL6 and Ceramide synthase 2 knockdown (data not shown) were performed like ELOVL1 knockdown in CCALD patients' fibroblasts. Both lipidomic and FA patterns in Figures 7 and 8 were consistent with compound concentration, IC_{50} and with the inhibition of FAs elongation starting in the first step in the cascade where ELOVL1 plays a major role, resulting in accumulation of the substrate in the first step (C20) and substantial reduction of the products of the last subsequent steps (C24, C26 and C28). The concordance between small-molecule inhibitor and genetic knockdown profiles confirms on-target ELOVL1 inhibition and rules out off-target effects on upstream (ELOVL6) or downstream (CerS2) pathway components. This mechanistic validation strengthens confidence in the therapeutic potential of these inhibitors.

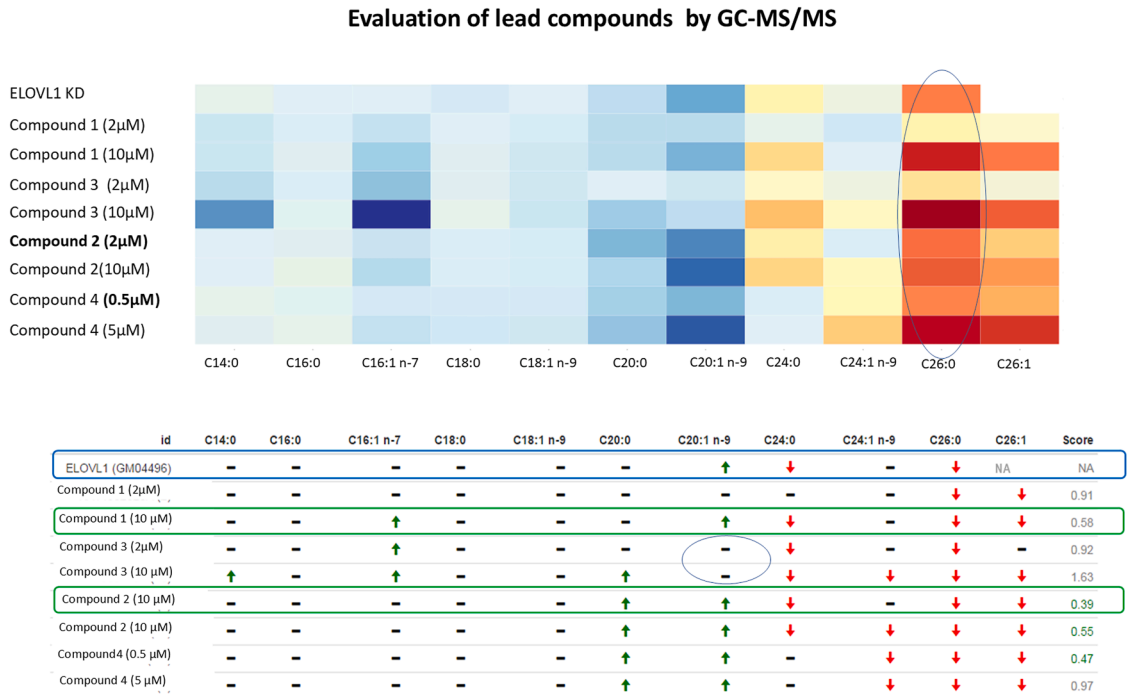

Figure 7. Evaluation of ELOVL1 inhibitors effect on Fatty Acids Level in cells by GC-MS/MS. Fatty acids analysis of patient fibroblasts demonstrates moderate reduction in C24:0 and C24:1 and significant reduction in C26:0 and C26:1 FAs with siRNA ELOVL1 knockdown and small-molecule inhibitors. Response is consistent with IC_{50} values and concentration of the active compound. The data is presented as a hit map on the top, and a diagram with arrows showing the direction of the change in the normalized levels of VLCFAs. Hit maps demonstrate that compounds action is in good agreement with the ELOVL1 KO signature: % Correlation between the ELOVL1 KO FAs profile (*top rows* on both hit map and the diagram) is listed in the last column of the diagram. Compounds 1 and 2 in Figure 7 are the same compounds as those used to generate lipid profiles shown in Figure 8. There is a good agreement between lipid profiles and fatty acids profile. The assay demonstrates that GC-MS remains a powerful tool for monitoring shifts in FA metabolism and confirmation of the mechanism of action of the active compound.

In vitro *platform for ELOVL1 inhibitor discovery*

Biomarkers discovery to support ELOVL1 small-molecule inhibitor drug discovery

Fatty acids and Lipidomics profiling presented in this manuscript in support of ELOVL1 inhibitor identification, lead optimization and characterization of compound's mechanism of action led us to the discovery of interesting trends in lipids and FAs abundance which may be specific to the phenotype of the X-ALD disease and its severity. It was expanded later and evolved into an extensive search for early XALD disease biomarkers to inform pre-clinical and clinical development. (Significant findings from that effort are summarized in a separate manuscript which is in press, JBC 2026).

Discussion

ALD is a devastating, rare neuromuscular disease with multiple manifestations and a very high unmet medical need. While for the cerebral form of the disease there are available treatments, bone marrow transplant and gene therapy, there are significant challenges and limitations for both approaches: both show efficacy if only applied at the early stage of the disease and both are associated with significant health risks. For AMN, the disease form in most ALD patients, there are no available approved treatment options; and the field is actively looking for transformative approaches to treat this devastating disease. We applied a substrate reduction therapy strategy shown to be efficacious in the clinic for Gaucher disease with approved small molecule treatments Zavesca (miglustat) (19) and Cerdelga (eliglustat) (20, 21). There are currently multiple clinical trials with SRT approach on small molecules for other rare diseases, including Fabry disease (venglustat) (22), Niemann-Pick type-C disease (miglustat) (23) and Pompe disease (MZE001) (24). Complementary to enzyme replacement therapy, substrate reduction therapy enables the development of CNS active small molecules with a great potential to be applied for the treatment of neurological diseases.

Adrenoleukodystrophy manifestations are caused by mutations in the ABCD1 transporter responsible for the transport of VLCFA to peroxisomes for degradation; these mutations result in the accumulation of VLCFA with C26:0 identified as a major cause of ALD pathology. VLCFA are synthetized by the ELOVL family of elongases, with known 7 family members in humans with diverse substrate specificity and localization. ELOVL1 is a rate-limiting and the single elongase catalyzing the synthesis of saturated C24:0 and C26:0 VLCFA, the hallmark of ALD; and represents an attractive SRT target for development of the treatment for all ALD phenotypes.

We developed a robust *in vitro* platform to initiate the hunt for small-molecule ELOVL1 inhibitors for X-ALD treatment. We established a variety of biochemical and cell-based assays to monitor ELOVL1 inhibitors' properties and inform medicinal chemistry efforts. Complementary, we developed a robust Lipidomics profiling platform that enables the development of cell-based assays and initiates the disease biomarkers' discovery. We also established robust methods for the detection of a wide range of VLCFAs by GC-MS, which were instrumental in ELOVL1 activity assessments in cells and tissues.

Selected Lipids	LOG10 (ratio)	Knockdown			Compound 1		Compound 2	
		ELOVL1	ELOVL6	CerS2	2uM	10uM	0.3uM	2uM
Sphingomyelin	SM16:1	-0.03	0.05	0.07	0.02	0.05	0.01	0.01
	SM18:1	0.07	0.04	0.06	0.01	0.15	0.06	0.22
	SM18	0.19	0.07	0.06	0.08	0.31	0.16	0.45
	SM20:1	0.25	0.02	0.07	0.15	0.59	0.32	0.72
	SM20	0.22	0.07	0.07	0.17	0.49	0.33	0.63
	SM22:1	0.04	0.06	0.07	0.11	0.27	0.16	0.26
	SM22	-0.04	0.09	0.07	0.07	0.04	0.12	0.11
	SM24:1	-0.11	0.13	0.11	0.01	-0.07	0.03	-0.08
	SM24	-0.18	0.12	0.11	-0.05	-0.25	-0.07	-0.17
	SM26:1	-0.24	0.17	0.16	-0.06	-0.3	-0.15	-0.28
	SM26	-0.23	0.18	0.14	-0.1	-0.4	-0.16	-0.22
LysoPC	LPC16:1	-0.01	0.02	-0.01	-0.03	0.34	0.05	0.08
	LPC16	-0.01	-0.06	-0.02	-0.02	0.2	-0.01	-0.01
	LPC18:1	0	-0.04	-0.01	-0.02	0.31	0.03	0.07
	LPC18	0.03	-0.01	0.03	0.01	0.2	0.02	0.05
	LPC20:1	0.05	0.02	0.05	-0.01	0.25	0.07	0.18
	LPC20	-0.03	0.14	0.13	0.03	0.31	-0.01	0
	LPC22:1	0.02	0.14	0.13	0.03	0.64	0.06	0.12
	LPC22	-0.09	0.13	0.1	0.05	0.42	0.01	0.03
	LPC24	-0.16	-0.02	0	-0.02	0.02	-0.16	-0.35
	LPC 26:1	-0.25	-0.03	0.03	-0.09	-0.12	-0.39	-0.71
	LPC 26	-0.24	0	-0.01	-0.15	-0.3	-0.35	-0.69
	LPC28:1	-0.21	0.04	0.03	-0.15	-0.25	-0.36	-0.59
	LPC28	-0.19	0.03	0.01	-0.16	-0.31	-0.39	-1.35
PC	PC(16:0/18:1)	-0.03	0.01	0.03	0	0.02	-0.01	-0.02
	PC(18:0/18:1)	0.01	-0.01	0.01	0	0.01	0	0.02
	PC(24:0/18:1)	-0.49	-0.04	0.06	-0.09	-0.57	-0.3	-0.8
	PC(26:0/16:0)	-0.63	-0.09	0.01	-0.26	-1	-0.46	-1.05
	PC(26:0/18:1)	-0.6	-0.08	0	-0.15	-0.8	-0.45	-1.01
Ceramide	Cer16	0.08	0.11	0.05	0.02	0.05	0.05	0.2
	Cer18:1	0.03	0.06	0.06	0.07	0.26	0.18	0.33
	Cer18	0.09	0.05	0.07	0.06	0.26	0.17	0.5
	Cer20	0.06	0.05	0.13	0.11	0.38	0.23	0.58
	Cer22:1	-0.05	0.09	0.12	0.09	0.3	0.17	0.31
	Cer22	-0.04	0.07	0.13	0.12	0.1	0.14	0.25
	Cer24:1	-0.13	0.12	0.14	0.04	0.02	-0.02	-0.1
	Cer24	-0.2	0.11	0.13	0.02	-0.3	-0.11	-0.22
	Cer26:1	-0.23	0.21	0.2	-0.08	-0.39	-0.26	-0.42
	Cer26	-0.21	0.21	0.17	-0.1	-0.59	-0.29	-0.39

LOG10 (ratio)	Knockdown			Compound 1		Compound 2	
	ELOVL1	ELOVL6	CerS2	2uM	10uM	0.3uM	2uM
SM20:1	0.25	0.02	0.07	0.15	0.59	0.32	0.72
SM20	0.22	0.07	0.07	0.17	0.49	0.33	0.63
SM24:1	-0.11	0.13	0.11	0.01	-0.07	0.03	-0.08
SM24	-0.18	0.12	0.11	-0.05	-0.25	-0.07	-0.17
SM26:1	-0.24	0.17	0.16	-0.06	-0.3	-0.15	-0.28
SM26	-0.23	0.18	0.14	-0.1	-0.4	-0.16	-0.22
LPC24	-0.16	-0.02	0	-0.02	0.02	-0.16	-0.35
LPC 26:1	-0.25	-0.03	0.03	-0.09	-0.12	-0.39	-0.71
LPC 26	-0.24	0	-0.01	-0.15	-0.3	-0.35	-0.69
LPC28	-0.19	0.03	0.01	-0.16	-0.31	-0.39	-1.35

Figure 8. Hit map of the ELOVL1 inhibitors MoA: Effects on Lipids. Lipidomics analysis of patient fibroblasts demonstrates reduction in C24- and C26-containing lipids with siRNA ELOVL1 knockdown and small-molecule inhibitors. Response consistent between lysoPC (diagnostic biomarker) and SM (screening readout). Hit maps showed that compound action is in good agreement with ELOVL1 KO signature and not with ELOVL6 or CerS2 signatures.

Two HTS campaigns were performed to find CNS-active ELOVL1 small molecule inhibitors for ALD treatment.

Hits from the biochemical HTS were rigorously validated using innovative biochemical and cell-based assays, aiding SAR analysis in medicinal chemistry. Lipidomics profiling of small-molecule ELOVL1 inhibitors was established to obtain the compounds' signature and aid in significant insights of compound elongase pathway profiles.

While our study demonstrates ELOVL1 inhibition through biochemical selectivity assays and comparison with ELOVL6 and CerS2 knockdowns, additional knockdown experiments for ELOVL3 and ELOVL7 would further strengthen the characterization of the ELOVL1-specific lipid signature and represent a valuable direction for future investigation.

Several promising leads were identified and tested in a variety of animal models. Although our lead compound did not achieve an acceptable safety profile, it showed a significant reduction of VLCFA including C26:0 in the brain and spinal cord of *ABCD1* knockout (KO) mice, the model for X-ALD (25). Analysis of all published data on ELOVL1 small molecule inhibitors highlights the challenges associated with modulating this target activity (26, 27). However, different chemical scaffolds have exhibited varying safety profiles and liabilities, thus suggesting that further optimization could improve the safety margin at efficacious doses.

It is worth noting that ELOVL1 inhibition potentially can benefit in other disease indications. ELOVL1's role was proposed in mediating the toxic activity of reactive astrocytes *via* toxic lipids containing VLCFAs; and it has been shown that astrocyte-specific knockout of ELOVL1 mitigates the astrocyte-mediated toxicity *in vitro* and *in vivo* model (28). This opens a new opportunity to consider ELOVL1 activity modulation by small-molecule inhibitors in neuro-inflammatory diseases.

In recent years, ELOVL1 gained a lot of interest as a potential therapeutic target for cancer. It has been shown that ELOVL1 level is significantly upregulated in several types of cancers, including colorectal (CRC) (29), breast (30) and hepatocellular carcinoma (HCC) cancers (31) and high ELOVL1 expression is associated with increased tumor growth, cancer cells proliferation, migration and survival. It had been hypothesized that ELOVL1 drives metastasis in melanoma cancers by modulating sphingolipid ceramides that are involved in apoptosis and cancer cell invasion; and inhibition of ELOVL1 potentially disrupts VLCFA-dependent survival pathways in cancer cells (32). Very recently, it was shown that ELOVL1 inhibition synergized with anti-PD1 to promote effective T cell response in resistant pancreatic and melanoma tumors (33). It was also observed that anti-PD1 therapy in patients with low ELOVL1 expression in $CD8^+$ tumor-infiltrating lymphocytes correlated with a better treatment outcome, opening an opportunity to improve the efficacy of the cancer immunotherapy by combining with ELOVL1 modulation (33, 34).

The *in vitro* biology methods described in this publication provide robust support for potential future research on the role of ELOVL1 in human health and diseases, and we hope this paper will aid researchers in developing a safer and more effective ELOVL1 inhibitor for ALD and cancer treatment.

Experimental procedures

Human elongase enzymes expression

ELOVL 1, 3, 6, and 7 were expressed using the Baculovirus system; full-length ELOVLs proteins were cloned into the pFastBac3 (or 5) vector with N-terminus His-Flag tags (BPS Biosciences).

ELOVL1 (aa 2–279(end)) NM_022821:

MHHHHHHGSSGDYKDDDDKGSSGENLYFQGSSGEAV
VNLYQEVMKHADPRIQGYPLMGSPLLMTSILLTYVYFVLS
LGPRIMANRKPFQLRGFMIVYNFSLVALSLYIVYEFLMSGW
LSTYTWRCDPVDYSNSPEALRMVRVAWLFLFSKFIELMDT
VIFILRKKDGQVTFLHVFHHSVLPWSWWWGVKIAPGGM
GSFHAMINSSVHVIMYLYYGLSAFGPVAQPYLWWKKHM
TAIQLIQFVLVSLHISQYYFMSSCNYQYPVIIHLIWMYGTIF
FMLFSNFWYHSYTKGKRLPRALQQNGAPGIAKVKAN

ELOVL3 (aa 2–270(end)) NM_152310:

MHHHHHHGSSGDYKDDDDKGSSGENLYFQGSSGVTA
MNVSHEVNQLFQPYNFELSKDMRPFFEEYWATSFPIALIY
LVLIAVGQNYMKERKGFNLQGPLILWSFCLAIFSILGAVR
MWGIMGTVLLTGGLKQTVCFINFIDNSTVKFWSWVFLL
SKVIELGDTAFIILRKRPLIFIHWYHHSTVLVYTSFGYKNK
VPAGGWFVTMNFGVHAIMYTYYTLKAANVKPPKMLPM
LITSLQILQMFVGAIVSILTYIWRQDQGCHTTMEHLFWS-
FILYMTYFILFAHFFCQTYIRPKVKAKTKSQ

ELOVL6 (aa 2–265(end)) NM_024090:

MHHHHHHGSSGDYKDDDDKGSSGENLYFQGSSGNMS
VLTLQEYEFEKQFNENEAIQWMQENWKKSFLFSALYAAF
IFGGRHLMNKRAKFELRKPLVLWSLTLAVFSIFGALRTGA
YMVYILMTKGLKQSVCDQGFYNGPVSKFWAYAFVLSKA-
PELGDTIFIILRKQKLIFLHWYHHITVLLYSWYSYKDMVA
GGGWFMTMNYGVHAVMYSYYALRAAGFRVSRKFAMF
ITLSQITQMLMGCVVNYLVFCWMQHDQCHSHFQNIFW
SSLMYLSYLVLFCHFFFEAYIGKMRKTTKAE

ELOVL7(aa 2–281(end)) NM_024930:

MHHHHHHGSSGDYKDDDDKGSSGENLYFQGSSGAFS
DLTSRTVHLYDNWIKDADPRVEDWLLMSSPLPQTILLGF
YVYFVTSLGPKLMENRKPFELKKAMITYNFFIVLFSVYMC
YEFVMSGWGIGYSFRCDIVDYSRSPTALRMARTCWLYYF
SKFIELLDTIFFVLRKKNSQVTFLHVFHHTIMPWTWWFG
VKFAAGGLGTFHALLNTAVHVVMYSYYGLSALGPAYQK
YLWWKKYLTSLQLVQFVIVAIHISQFFFMEDCKYQFPVFA
CIIMSYSFMFLLLFLHFWYRAYTKGQRLPKTVKNGTCKN
KDN

ELOVL1b zebrafish (aa 1–320(end)) NM_001328594.

MLETVKDRVLEAYGSLLAARDPRLKDYPLMESPFSMTA
ILL-
AYLFFVLYAGPKFMANRKPFQLKEAMIIYNLSLVGLSAYIV
YEFLMSGWATGYTWRCDPCDYSNSPQGLRMARVAWLF
LFSKFIELMDTVFFVLRKKHSQITFLHIFHHSFMPWTWW
WGVSIVPGGMGSFHAMVNSCVHVIMYFYYGLSAAGPRF
QKFLWWKKYMTAIQLTQFVLVSLHVSQWYFMESCDFQ
VPVIIHLIWLYGTFFFVLFSNFWYQAYIKGKRLPKNTQET
TKTNGSTIVTNGSSGVSNGHAIHENGLSNGKKHHENGN

ALNGKMKKAGSMVSKGEELFTGVVPILVELDGDVNGH
KFSVSGEGEGDATYGKLTLKFICTTGKLPVPWPTLVTTLT
YGVQCFSRYPDHMKQHDFFKSAMPEGYVQERTIFFKDDG
NYKTRAEVKFEGDTLVNRIELKGIDFKEDGNILGHKLEYN
YNSHNVYIMADKQKNGIKVNFKIRHNIEDGSVQLADHYQ
QNTPIGDGPVLLPDNHYLSTQSKLSKDPNEKRDHMVLLEF
VTAAGITLGMDELYKHHHHHHHH

All ELOVL proteins were expressed in Sf9 insect cells by infection of 1 mL of baculovirus (titer 3–5*10^8-1*10^9 pfu/mL) to 1 L of cultured media (Expression Systems, ESF 921) and the cells were harvested 72 h later with cell viability >75 to 80%. Average cell pellet weight was 7 to 15*g* per 1 L of Sf9 cells (Expression Systems, 94-001S) culture. Cells were washed with PBS buffer (Gibco, 20012) and stored at −80 °C in 50 mL conical Falcon tubes (Corning, 352070).

ELOVL microsomes preparation

During the preparation of microsomes, all steps were carried out in a chilled environment.

Pellet of insect cells expressing the ELOVL proteins (pellet size ranging from 15-35*g*/2L culture) kept in 50 mL Falcon tube (Corning, 352070) at −80 °C was thawed in a cold water bath at 4 °C while spinning; and when completely thawed added to 200 mL of prechilled microsome buffer (50 mM HEPES pH 7.5 (Sigma, H0887), 25 mM potassium chloride(Sigma, P3911), 0.25 M sucrose (Sigma, S0389), 1 tablet per 50 mL protease inhibitor (Roche, 4693132001), 0.1 mM sodium orthovanadate (Sigma, S6508), 0.1 mM beta-glycerol phosphate (Sigma, G6251), and 20% glycerol (Sigma, G2025). Cell suspension was next sonicated on ice using a probe sonicator (Branson) with a horn tip. Suspension was spun down at 10,000*g* (Beckman, J-30I) for 10 min at 4 °C in 6 prechilled Nalgene round-bottom tubes followed by supernatant spin down at 100,000*g* (Beckman, J-30I) for 1 h at 4 °C in Beckman round-bottom polycarbonate tubes (Beckman Coulter, 357000). The pellets were resuspended in 3 mL of microsome buffer, and aliquots were stored at −80 °C in Eppendorf tubes.

ELOVL1 expression and purification

To generate detergent-purified ELOVL1 protein, full-length ELOVL1 was cloned into pFastBac1 as a C-terminal fusion with enhanced GFP followed by a C-terminal 8xHis tag, and expressed in Sf9 insect cells for 48 h at 27 °C. Cells were pelleted, resuspended in 50 mM Tris pH 7.4, 200 mM NaCl, 1% glycerol plus protease inhibitors, and frozen at −80 °C. For purification, cells were thawed in purification buffer (25 mM HEPES pH 7.4 (Sigma, H0887), 150 mM NaCl (Sigma, S6546), 10% glycerol (Sigma, G2025)), and the membrane fraction purified by successive centrifugation at 4500*g* and 100,000*g*. Protein was solubilized for 2.5 h at 4 °C in solubilization buffer (Purification buffer with 1.5% (w/v) beta-dodecyl maltoside (DDM, Sigma, D4641) and 0.3% (w/v) cholesterol hemisuccinate (CHS, Sigma, C6013), followed by pelleting of insolubilized material. Solubilized ELOVL1-eGFP was purified by Ni-NTA and size exclusion chromatography using a Superdex S200 10/30 Gl column (GE Healthcare) equilibrated in chromatography buffer (purification buffer with 0.04% (w/v) DDM, 0.008% (w/v) CHS), concentrated to 2 mg/mL, flash frozen, and stored at −80 °C until use.

Elongase activity assays using microsomes

The elongase microsomal assay was performed in three sequential steps: biochemical reaction, hydrolysis, and fatty acid extraction.

In human ELOVL1 enzyme activity assay: (1) 15 µl of microsomes (75 µg/mL, prepared in house) was preincubated with 15ul of substrate mixture containing 10 mM d4C22-CoA (Avanti Research, custom labeled), 350 nM Malonyl-CoA (Sigma, M4263), 250 mM NADPH (Sigma, N7785) at room temperature for 90 min in a 384-well Waters plate (Waters, 186002631) using assay buffer ((50 mM HEPES pH 6.8 (Sigma, H0887), 5 mM rotenone (Sigma, 557368), 10 mM BSA (Sigma, A8806), 150 mM NaCl(Sigma, S6546), 0.1 mM MgCl2 (Sigma, M1028), 0.1 mM CaCl2 (Fluka, 21114). (2) For the in-plate hydrolysis, 15 µL of 7.5 N KOH (Sigma, 60370) was added to each well, plate was sealed, centrifuged, and samples were incubated at 80 °C for 3 h (3) For fatty acid extraction, 50 µL of acetonitrile (Millipore Sigma, Supelco AX0156) was added to each well, plate was sealed and centrifuged at 3000*g* for 1 minute. Plates were then loaded onto the LX4-TSQ Quantiva system (Thermofisher) and only the top layer of the samples was injected for MS measurement, monitoring the elongation of d4C22 to d4C24.

Human ELOVL3 biochemical assay was performed in a manner analogous to that of the ELOVL1 assay with several modifications: in step (1) – microsome concentration was 30 µg/mL; substrate mixture was 7.5 mM d4stearoyl-CoA (Avanti Polar Lipids, custom labeled), 2.5 mM Malonyl-CoA (Sigma, M4263), 250 mM NADPH (Sigma, N7785) and incubation time was 60 min. In Step (2), the KOH concentration used was 0.5 N, and the hydrolysis reaction was performed at room temperature for 30 min. In step (3) the elongation of d4C18 to d4C20 was monitored.

Human ELOVL7 enzyme activity assay was performed using the protocol analogous to the ELOVL3 assay, with the exception that in step (1) 1 µM Malonyl CoA (Sigma, M4263) was used in the substrate mixture.

Human ELOVL6 biochemical assay was performed in a manner analogous to ELOVL3 assay with several modifications: in step (1) – microsome concentration was 20 µg/mL; substrate mixture was 5 mM (12) C-Palmitoyl- CoA (Sigma 655716), 5 mM ^{13}C-Malonyl-CoA (Sigma, 655759), 300 mM NADPH (Sigma, N7785). In step (2) KOH concentration used was 2.5 N and hydrolysis reaction was 60 min. In step (3) the elongation of 13C-C16 to 13C-C18 was monitored.

Zebrafish enzyme activity assay followed a protocol analogous to that of human ELOVL1 assays with several modifications: in step (1) – microsome concentration was 120 mg/mL; 10 mM d4C22-CoA, and 1 mM Malonyl-CoA were used in substrate mixture. Microsomes were isolated from Sf9

insect cells (Expression Systems, 94-001S) overexpressing zebrafish ELOVL1b.

ELOVL1 elongase activity assays using purified enzyme in proteoliposomes

Purified ELOVL1 activity assay in proteoliposomes was performed in analogous to the human ELOVL1 microsomal assay manner with prior treatment of the enzyme and several modifications. Palmitoyl-2-oleoyl-sn-glycero-3-phosphocholine (POPC, Avanti Research, 850457) was used to make proteoliposomes with purified ELOVL1 protein: POPC was transferred to a glass vial to evaporate chloroform and then reconstituted with assay buffer ((50 mM HEPES pH 6.8 (Sigma, H0887), 5 mM rotenone (Sigma, 557368), 10 mM BSA (Sigma, A8806), 150 mM NaCl(Sigma, S6546), 0.1 mM MgCl2 (Sigma, M1028), 0.1 mM CaCl2 (Fluka, 21114) to 10 mg/mL. The mixture was vortexed, which resulted in a milky white dispersion. It was further incubated at 50 °C for 1 h while being sonicated until the liposome dispersion becomes clear. Then the liposomes were cooled on ice for 5 min, and finally, 100 μL of purified ELOVL1 protein was added to 20 μL of 10 mg/mL liposomes (5:1 ratio), mixing 3 × 20 by pipetting on ice for 15 min.

Using proteoliposomes, the ELOVL1 activity assay was carried out similarly to the microsomal assay with the following exceptions: in step (1), the proteoliposome concentration was 8 μg/mL; 10 μM d4C22-CoA and 5 μM Malonyl-CoA were used in the substrate mixture. (2) Reaction was stopped by adding 70 μL of citrate buffer pH 5.0. (3) The elongation of d4C22 to three-keto-d4C24 was monitored.

Cell-based assay to study ELOVL1 inhibitors in human patients' fibroblasts

Human patient fibroblasts isolated from a 6-year-old Caucasian male with elevated C26 VLCFA levels (Coriell Institute, CCALD GM-04496) were plated to 384-well cell assay plates (Corning Cellbind, 3770) at 750 cells per well in 50 uL DMEM media (Gibco, 10566) with 10% FBS (Gibco, 16000-044) and 1% penicillin-streptomycin (Gibco, 15-140); and incubated for 72 h at 37 °C in the absence or presence of compound dispensed in a ten-point dose response manner with three-fold dilutions from 10 μM down to 0.5 nM final concentrations (50 nl per concentration/well) using Echo 655 Liquid Handler (Beckman 001–16080). After washing the plates with 1xPBS (Gibco, 20012) twice, the residual PBS volume was removed, and the plates were dried in a biosafety cabinet. Plates were either heat-sealed and frozen at −20 °C for future analysis or immediately underwent a lipids extraction procedure: To each well was added 85 μL of a 1:1 acetonitrile/methanol (MilliporeSigma, Supelco AX0156),(MilliporeSigma, MX0488P-1) solution with 0.1 mM phosphatidylcholine (PC) C17:0 (Avanti, 850360P) and 0.1 mM sphingomyelin C17:0 standards (Avanti, 860585P) for normalization. The plates were centrifuged for 5 min at 3000 rpm and 75 μL of the cell extraction was transferred to a 384-well assay plate (Waters, 186002631) using the Apricot iPipette. The plates were heat-sealed (Agilent PlateLoc) and analyzed on the Rapidfire (Agilent) API5000 (Sciex) MS/MS system to determine sphingomyelin C26:0 to C22:0 ratio.

Mouse cell-based assay

Mouse cell-based assay was performed using an assay analogous to human cell-based assays with few modifications: mouse *ABCD1* knockout fibroblasts (generated in-house) were plated to 384-well cell assay plates (Corning Cellbind, 3770) at 750 cells per well and incubated for 72 h at 37 °C in the absence or presence of compound, following the human cell-based assay protocol to determine sphingomyelin C26:0 to C22:0 ratio.

Species-specific (rat, dog, minipig) cell-based assays

Rat liver fibroblasts (BRL3A, ATCC), canine kidney epithelial cells (MDCKII, Sigma) and minipig kidney fibroblasts (MPK, ATCC) were plated at 1500, 400, and 2500 cells per well, respectively, and incubated for 72 h at 37 °C in the absence or presence of compound following the human cell-based assay protocol to determine sphingomyelin C26:0 to C22:0 ratio.

Cell viability assays

All assays were developed by using ATPlite 1step Luminescence Assay (Revvity, 6016731) in 384-well plate format.

In human cell viability assay, patient fibroblasts (750 cells/well) were incubated in the absence or presence of compounds for 72 h at 37 °C. After removing the media from the plates, 20 μL/well of ATPLite 1step reagent was added using the Multidrop dispenser or multichannel pipette. The plates were centrifuged for 30 s at 1000 rpm, and the luminescence signal was read on the Pherastar (BMG) plate reader.

In mouse, rat, dog and minipig cell viability assay: Cells (750 mouse *ABCD1* knockout cells/well, 1500 BRL3A rat cells/well, 2500 minipig MPK cells/well, and 400 MDCKII dog cells) were incubated in the absence or presence of compounds for 72 h at 37 °C following the human assay protocol till the last step where the luminescence signal was read on the Pherastar (BMG) plate reader.

siRNA-mediated ELOVL1 knockdown in ABCD1 KO background

The synthetic small interfering RNA (siRNA) system from the "Dharmacon siRNA solution" was used in this study. The DharmaFECT three Transfection Reagent (Horizon Discovery, T-2003–03) was selected based on its ability to achieve highly effective transfection level in X-ALD fibroblasts (Coriell Institute, GM-04496 and GM-03348) at low concentrations with minimal toxicity by optimized siRNA delivery. siRNA sequences were obtained directly from the manufacturer. ON-TARGETplus siRNAs ELOVL1(L-009355–01–0005) and GAPDH control pool (D-001830-10-05) were used due to their high specificity and reduced off-target effects.

Detailed procedure: 25k-30k fibroblasts (Coriell Institute, GM-04496 and GM-03348) per well were seeded on a 6-well plate (Costar CLS3516) and incubated overnight at 37° C to allow the cells to adhere and grow. Next day, the working solutions of transfection reagents were prepared: 1.5 μL of 20 μM siRNA stock was diluted in 198.5 μL sodium free medium Opti-MEM (Gibco 11058-021) in tube 1 (50 mL Falcon tubes, Corning, 352070); and 2.5 μL of transfection reagent DharmaFECT three was diluted in 197.5 μL sodium free medium Opti-MEM (Gibco 11058-021) in tube 2 (50 mL Falcon tubes, Corning, 352070); tube 1 and tube 2 were incubated at room temperature (RT) for 5 min. Then transfection reagents were combined in tube 1 and incubated for 20 min at RT, followed up by the addition of 800 μL of complete culture media, Minimum Essential Medium (Corning, 10-009-CV) with 15% Fetal Bovine Serum (Gibco, A5670402). Following gentle mixing, 1 mL of the transfection mixture was dispensed into each well of the 6-well plate (Costar, 3516) containing fibroblasts. Ensuring uniform distribution of the transfection reagent across each well was essential for consistent transfection efficiency.

siRNA was incubated with fibroblasts for 24 to 72 h at 37 °C followed by assessment of transfection efficiency and toxicity.

Global lipidomics profiling

The fibroblasts (0.5million) in microcentrifuge tubes were removed from the −80 °C freezer and allowed to thaw on ice, followed by the addition of 1 mL extraction solution containing a mixture of internal standard lipid (1:1 acetonitrile/methanol, acetonitrile (MilliporeSigma, Supelco AX0156), methanol (Fisher, A456) lipids standards, see Table S1, Avanti Research).

The samples were vortexed (10 min) and then centrifuged (10 min, 8000 rpm). The supernatant was carefully transferred (900 μL) to a Waters MS vial and then dried under the nitrogen evaporator until all of the solvent had been evaporated. The lipid extract was reconstituted into 90 μL of 7:3 acetonitrile/methanol solution containing an additional internal standard, stably labeled lysophosphatidylcholine (10 ng/mL d4-LPC, Avanti Research, 860389). The samples were mixed well for MS analysis.

Lipids were separated with Waters ACQUITY BEH HILIC, (1.7 μm, 2.1 × 150 mm) column at a constant temperature of 30 °C while the autosampler maintained the temperature of 8 °C. The analytes were gradually eluted using a mixture of mobile phase A (MPA): 5 mM Ammonium Acetate in 96:2:2:0.1 acetonitrile:methanol:water:acetic acid, and mobile phase B (MPB): 98:2:0.1 methanol:water:acetic acid, 5 mM ammonium acetate.

The gradient starts with 95% MPA, moves to 40% MPA in 20 min, maintaining a flow rate of 0.3 mL/min. Following the equilibration phase, each sample was administered in a 5 μL injection.

The data is collected by Thermo QExactive Plus mass spectrometry, with spray voltages of 3.0 kV (Positive and negative switch modes). The sheath gas was set to 30 arbitrary units, and the auxiliary gas was set to 6 arbitrary units. The capillary temperature was 300 °C. The Orbitrap analyzer performed a scan over the mass range of 300 to 1500 m/z with a resolution of 70,000 in full-scan mode. In the data-dependent acquisition (DDA) MS/MS experiment, we used the HCD (higher-energy collisional dissociation) scan technique. The energy of the normalized collision was 30 eV.

Total fatty acid measurement method in human CCALD fibroblasts and mouse ABCD1 knockout fibroblasts

A low-throughput method was developed to confirm that compounds are lowering C26 total fatty acids and not just the sphingomyelin C26 level.

1.5 mL per well of complete media (DMEM (Gibco, 10566) with 10% FBS (Gibco, 16000–044) and 1% penicillin-streptomycin (Gibco, 15–140) containing DMSO (at 0.5% final concentration) or compound (at various concentrations, typically 10 mM final concentration) was added to a 6-well plate (Costar, 3516) followed by addition of 125,000 cells/well of either human CCALD fibroblasts or mouse *ABCD1* knockout cells in 1.5 mL of complete media. Plates were gently swirled to mix the contents and incubated for 72 h at 37 °C when the cells reached 100% confluency. Media was aspirated off the wells and cells were washed with 3 mL 1x PBS (Gibco, 20012). 0.5 mL of trypsin (Gibco, 252200) per well was added to harvest the cells. The plate was put in the CO2 incubator (37 °C) for 5 to 10 min until the cells were dislodged. After gently tapping the plate, the cells were collected in 1.5 mL centrifuge tubes (Eppendorf, 022363204). Wells were rinsed with 0.5 mL PBS, and the wash was collected in the tubes. The tubes were then spun down on a benchtop centrifuge for 2 minutes at 3000 rpm. Supernatant was removed by aspiration. Another 0.5 mL of PBS was added to the tubes which were then centrifuged again for 1 min at 3000 rpm. Supernatant was aspirated. The pellets were frozen at −80 °C until subjected to GCMS analysis to determine the total fatty acid content (Agilent triple quadrupole). A total of 35 fatty acids were quantified from C11:0 to C26:0 including 14 saturated, 8 mono- and 12 poly-unsaturated fatty acids.

De novo VLCFA synthesis monitoring using labeled substrates

$^{13}C_6$-C22 labeled substrate (docosanoic acid (1,2.3.4.5.6-^{3}C6), Cambridge Isotope Labs Inc., CML-99909–0) was also sometimes used to monitor elongation and fatty acid levels using GCMS analysis (Fig. S6). The $^{13}C_6$-C22-stock in ethanol was sonicated and heated immediately before use due to insolubility at room temperature in ethanol. The labeled substrate was diluted to 3 mM in cell culture media. Then, 0.1% DMSO and compound dilutions were prepared in 3 mM $^{13}C_6$-C22 labeled substrate and added to a 6-well plate (Costar, 3516). 125,000 cells/well were added in 1.5 mL of complete media. Plates were gently swirled to mix the contents and incubated for 72 h at 37 °C when the cells reached 100% confluency. Media was aspirated off the wells and cells were washed with 3 mL 1x PBS buffer (Gibco, 20012). 0.5 mL of trypsin (Gibco, 252200) per well was added to harvest the

cells. The plate was put in the CO2 incubator (37 °C) for 5 to 10 min until the cells were detached. After gently tapping the plate, the cells were collected in 1.5 mL centrifuge tubes. Wells were rinsed with 0.5 mL PBS, and the wash was collected in the tubes. The tubes were then spun down on a benchtop centrifuge for 2 minutes at 3000 rpm. Supernatant was removed by aspiration. Another 0.5 mL of PBS was added to the tubes, which were then centrifuged again for 1 min at 3000 rpm. Supernatant was aspirated. The pellets were frozen at −80 °C until subjected to GCMS analysis to determine the total fatty acid content.

Measurement of very long-chain fatty acids (VLCFA)

Cell pellets were thawed, and 50 mg of sample was weighed out. Fatty acid profiling was performed for total fatty acids, including free fatty acids and bound fatty acids after derivatization with methanol (Fisher, A456) in the presence of Boron Trifluoride (BF3) as a catalyst. The derivatization products, Fatty Acid Methyl Ester (FAME), were analyzed by Agilent Triple Quadrupole GC-MS/MS (7000C). A total of 35 fatty acids were analyzed by this method, including saturated, monounsaturated, and polyunsaturated fatty acids.

Cell lysates were transferred into a digestion tube, and 2 mL BF3 in Methanol (Trifluoroborate (BF3) 14% in methanol, Sigma-Aldrich PN B1252) and 40 µL of internal standard solution (250 µg/mL of C19:0 methyl ester with 1200 µg/mL Butylated Hydroxytoluene (BHT, Sigma Aldrich PN W218405) in heptane) were added. The samples were then digested on a heatblock at 100 °C for 1 h. Once cooled, 2 mL heptane and 4 mL deionized water were added for extraction. Sample extracts were analyzed undiluted and diluted 1:50 with diluent by GC-MS/MS. Calibration standards for all 35 fatty acid methyl esters (FAMEs) were prepared in heptane with the internal standard (C19:0 methyl ester). The analysis method employed was capillary gas chromatography with positive chemical ionization (PCI) and detection with a triple-quadrupole mass spectrometer (GC-MS/MS) by Multiple Reaction Mode (MRM). The GC separation was achieved using HP-INNOWax GC Column, 20 m, 0.18 mm ID, 0.18 um film thickness (Agilent 19091N-577). Methane was used as a reagent gas for chemical ionization.

Fatty acids were quantified using calibration curves that consisted of at least 5 concentration levels. Calibration curves were established by a regression of either linear or quadratic fit with or without 1/x weighing, and required a minimum R2 greater than 0.99. The back-calculated calibration standards were within 25% of the nominal values. Data was processed using MassHunter 8.0 software.

Statistical analysis

Data are presented as mean ± standard deviation (*SD*) from three independent biological replicates. Statistical significance was assessed using two-tailed unpaired Student's *t* test for comparisons between two groups. *p*-values are indicated as follows: $^{*}p < 0.05$, $^{**}p < 0.01$. Statistical analyses were performed using GraphPad Prism ten. Assay quality was evaluated using the Z'-factor, a statistical metric that incorporates the means (μ_p, μ_n) and standard deviations (σ_p, σ_n) of the positive and negative control populations. The positive control consisted of a reference inhibitor at a concentration that produced complete (100%) inhibition of enzymatic or cell-based activity, whereas the negative control consisted of DMSO, yielding 0% inhibition. The Z'-factor was calculated using the equation:

$$Z' = 1 - 3 \setminus (\sigma_{-}(p) + \sigma_{-}(n)) / |\mu_{-}(p) - \mu_{-}(n)|.$$

Data availability

Due to the significant volume of the data generated in the studies described in this publication, it is not feasible to include all of it as part of the submission. If there is interest in data beyond summaries provided in the paper and the associated supporting information, it can be provided in response to a reasonable request.

Supporting information—This article contains supporting information [18].

Acknowledgments—The authors would like to thank Dr James Lily and Dr John Leonard for the support and guidance on the project, Dr Cary Valley, Dr Erica Walsh-Michel and Minjia Zhang for their assistance in elongase assay development, Dr Stephan Kemp and Dr Marc Engelen (AMC, University of Amsterdam, the Netherlands) for great discussions on ELOVL1 as a target for X-ALD and data reviewing, Dr Florian Eichler (MGH) for fruitful discussions on X-ALD disease, Prof. Stroud (UCSF) for providing protocols for ELOVL1 protein expression and purification, Dr Aurora Pujol for guidance on the project, Jill Gregory for leading the compound management team, and ELOVL1 small-molecule inhibitor for X-ALD Sanofi Team for the great work, support, and inspiration.

Author contributions—L. G., Z. D., B. T., M. K., D. W., S. H., M. H., B. L., A. B., G. A., M. C., Z. Z., B. F., and A. K. writing – review & editing; L. G., Z. D., B. T., T. G., D. W., S. H., M. H., B. L., A. B., G. A., M. C., Z. Z., and A. K. validation; L. G., Z. D., B. T., M. K., D. W., S. H., B. L., G. A., and A. K. software; L. G., Z. D., T. G., P. L., D. W., M. H., B. L., A. B., G. A., M. C., Z. Z., and A. K. resources; L. G., Z. D., B. T., P. L., D. W., S. H., M. H., B. L., A. B., G. A., M. C., Z. Z., B. F., and A. K. investigation; L. G., Z. D., B. T., M. K., D. W., M. H., B. L., G. A., M. C., Z. Z., and A. K. formal analysis; L. G., Z. D., B. T., M. K., D. W., S. H., M. H., B. L., G. A., Z. Z., and A. K. data curation, L. G., P. L., M. C., B. F., and A. K. conceptualization; B. T., M. K., D. W., S. H., G. A., Z. Z., and A. K. visualization; P. L. funding acquisition; T. G. writing–original draft; T. G., D. W., G. A., M. C., B. F., and A. K. supervision; P. L. project administration; P. L., D. W., A. B., G. A., M. C., B. F., and A. K. methodology.

Funding and additional information—This work was fully funded by Sanofi.

Conflict of interest—The authors declare that they have no conflicts of interest with the contents of this article: All authors are/were

employees of Sanofi and may own stock/stock options in the company.

Abbreviations—The abbreviations used are: ABCD1, gene, encoding a membrane transporter protein belonging to the ATP-binding cassette (ABC), subfamily D involved in the peroxisomal beta-oxidation of very long-chain fatty acids; ABCD1 KO, ABCD1 knockout; ALDP, adrenoleukodystrophy protein; AMN, adrenomyeloneuropathy; ATP, adenosine triphosphate; CALD, cerebral ALD; ELOVL, elongation of very long chain fatty acids protein family; ELOVL1, elongation of very long-chain fatty acids protein 1 family member which is a major contributor in elongation of C20-C26 saturated and monounsaturated acyl-CoA; HSCT, hematopoietic stem cell transplantation; LC, liquid chromatography; MS, Mass Spectrometry; VLCFA, Very long chain fatty acid; VLCFAs, Very long-chain fatty acids; WT, Wild type; X-ALD, X-Linked Adrenoleukodystrophy.

References

1. Mosser, J., Douar, A. M., Sarde, C. O., Kioschis, P., Feil, R., Moser, H., *et al.* (1993) Putative X-linked adrenoleukodystrophy gene shares unexpected homology with ABC transporters. *Nature* **361**, 726–730
2. van Geel, B. M., Bezman, L., Loes, D. J., Moser, H. W., and Raymond, G. V. (2001) Evolution of phenotypes in adult male patients with X-linked adrenoleukodystrophy. *Ann. Neurol.* **49**, 186–194
3. Engelen, M., Kemp, S., de Visser, M., van Geel, B. M., Wanders, R. J., Aubourg, P., *et al.* (2012) X-linked adrenoleukodystrophy (X-ALD): clinical presentation and guidelines for diagnosis, follow-up and management. *Orphanet J. Rare Dis.* **7**, 51
4. Engelen, M., Barbier, M., Dijkstra, I. M., Schur, R., de Bie, R. M., Verhamme, C., *et al.* (2014) X-linked adrenoleukodystrophy in women: a cross-sectional cohort study. *Brain* **137**, 693–706
5. Jangouk, P., Zackowski, K. M., Naidu, S., and Raymond, G. V. (2012) Adrenoleukodystrophy in female heterozygotes: underrecognized and undertreated. *Mol. Genet. Metab.* **105**, 180–185
6. Husebye, E. S., Pearce, S. H., Krone, N. P., and Kampe, O. (2021) Adrenal insufficiency. *Lancet* **397**, 613–629
7. Aubourg, P., Blanche, S., Jambaque, I., Rocchiccioli, F., Kalifa, G., Naud-Saudreau, C., *et al.* (1990) Reversal of early neurologic and neuroradiologic manifestations of X-linked adrenoleukodystrophy by bone marrow transplantation. *N. Engl. J. Med.* **322**, 1860–1866
8. Shapiro, E., Krivit, W., Lockman, L., Jambaque, I., Peters, C., Cowan, M., *et al.* (2000) Long-term effect of bone-marrow transplantation for childhood-onset cerebral X-linked adrenoleukodystrophy. *Lancet* **356**, 713–718
9. Miller, W. P., Rothman, S. M., Nascene, D., Kivisto, T., DeFor, T. E., Ziegler, R. S., *et al.* (2011) Outcomes after allogeneic hematopoietic cell transplantation for childhood cerebral adrenoleukodystrophy: the largest single-institution cohort report. *Blood* **118**, 1971–1978
10. Cartier, N., Hacein-Bey-Abina, S., Bartholomae, C. C., Veres, G., Schmidt, M., Kutschera, I., *et al.* (2009) Hematopoietic stem cell gene therapy with a lentiviral vector in X-linked adrenoleukodystrophy. *Science* **326**, 818–823
11. Eichler, F., Duncan, C., Musolino, P. L., Orchard, P. J., De Oliveira, S., Thrasher, A. J., *et al.* (2017) Hematopoietic stem-cell gene therapy for cerebral adrenoleukodystrophy. *N. Engl. J. Med.* **377**, 1630–1638
12. van Roermund, C. W., Visser, W. F., Ijlst, L., van Cruchten, A., Boek, M., Kulik, W., *et al.* (2008) The human peroxisomal ABC half transporter ALDP functions as a homodimer and accepts acyl-CoA esters. *FASEB J.* **22**, 4201–4208
13. Singh, I., Moser, A. E., Moser, H. W., and Kishimoto, Y. (1984) Adrenoleukodystrophy: impaired oxidation of very long chain fatty acids in white blood cells, cultured skin fibroblasts, and amniocytes. *Pediatr. Res.* **18**, 286–290
14. Wanders, R. J., van Roermund, C. W., van Wijland, M. J., Heikoop, J., Schutgens, R. B., Schram, A. W., *et al.* (1987) Peroxisomal very long-chain fatty acid beta-oxidation in human skin fibroblasts: activity in Zellweger syndrome and other peroxisomal disorders. *Clin. Chim. Acta* **166**, 255–263
15. Moser, H. W., Moser, A. B., Frayer, K. K., Chen, W., Schulman, J. D., O'Neill, B. P., *et al.* (1981) Adrenoleukodystrophy: increased plasma content of saturated very long chain fatty acids. *Neurology* **31**, 1241–1249
16. Kemp, S., and Wanders, R. (2010) Biochemical aspects of X-linked adrenoleukodystrophy. *Brain Pathol.* **20**, 831–837
17. Wang, X., Yu, H., Gao, R., Liu, M., and Xie, W. (2023) A comprehensive review of the family of very-long-chain fatty acid elongases: structure, function, and implications in physiology and pathology. *Eur. J. Med. Res.* **28**, 532
18. Ferrero, E., Vaz, F. M., Cheillan, D., Brusco, A., and Marelli, C. (2025) The ELOVL proteins: very and ultra long-chain fatty acids at the crossroads between metabolic and neurodegenerative disorders. *Mol. Genet. Metab.* **144**, 109050
19. Ficicioglu, C. (2008) Review of miglustat for clinical management in gaucher disease type 1. *Ther. Clin. Risk Manag.* **4**, 425–431
20. *Clinical Review Report: Eliglustat (Cerdelga): (Sanofi Genzyme): Indication: Gaucher Disease Type 1*. (2017). Canadian Agency for Drugs and Technologies in Health, Ottawa (ON)
21. Poole, R. M. (2014) Eliglustat: first global approval. *Drugs* **74**, 1829–1836
22. Deegan, P. B., Goker-Alpan, O., Geberhiwot, T., Hopkin, R. J., Lukina, E., Tylki-Szymanska, A., *et al.* (2023) Venglustat, an orally administered glucosylceramide synthase inhibitor: assessment over 3 years in adult males with classic fabry disease in an open-label phase 2 study and its extension study. *Mol. Genet. Metab.* **138**, 106963
23. Patterson, M. C., Mengel, E., Vanier, M. T., Moneuse, P., Rosenberg, D., and Pineda, M. (2020) Treatment outcomes following continuous miglustat therapy in patients with Niemann-Pick disease type C: a final report of the NPC registry. *Orphanet J. Rare Dis.* **15**, 104
24. Ullman, J. C., Mellem, K. T., Xi, Y., Ramanan, V., Merritt, H., Choy, R., *et al.* (2024) Small-molecule inhibition of glycogen synthase 1 for the treatment of pompe disease and other glycogen storage disorders. *Sci. Transl. Med.* **16**, eadf1691
25. Huang, J. Y., Freed, B., Hanus, M., Keefe, K., Chiang, M. S. R., Brezzani, A., *et al.* (2025) Elovl1 inhibition reduced very long chain fatty acids in a mouse model of adrenoleukodystrophy. *iScience* **28**, 113248
26. Come, J. H., Senter, T. J., Clark, M. P., Court, J. J., Gale-Day, Z., Gu, W., *et al.* (2021) Discovery and optimization of pyrazole amides as inhibitors of ELOVL1. *J. Med. Chem.* **64**, 17753–17776
27. Boyd, M. J., Collier, P. N., Clark, M. P., Deng, H., Kesavan, S., Ronkin, S. M., *et al.* (2021) Discovery of novel, orally bioavailable pyrimidine ether-based inhibitors of ELOVL1. *J. Med. Chem.* **64**, 17777–17794
28. Guttenplan, K. A., Weigel, M. K., Prakash, P., Wijewardhane, P. R., Hasel, P., Rufen-Blanchette, U., *et al.* (2021) Neurotoxic reactive astrocytes induce cell death *via* saturated lipids. *Nature* **599**, 102–107
29. Hama, K., Fujiwara, Y., Hayama, T., Ozawa, T., Nozawa, K., Matsuda, K., *et al.* (2021) Very long-chain fatty acids are accumulated in triacylglycerol and nonesterified forms in colorectal cancer tissues. *Sci. Rep.* **11**, 6163
30. Yamashita, Y., Nishiumi, S., Kono, S., Takao, S., Azuma, T., and Yoshida, M. (2017) Differences in elongation of very long chain fatty acids and fatty acid metabolism between triple-negative and hormone receptor-positive breast cancer. *BMC Cancer* **17**, 589
31. Qin, L., Song, C. Z., Yuan, F. Y., Wang, X. F., Yang, Y., Ma, Y. F., *et al.* (2024) ELOVL1 is upregulated and promotes tumor growth in hepatocellular carcinoma through regulating PI3K-AKT-mTOR signaling. *Heliyon* **10**, e34961
32. Du, A., Wang, Z., Huang, T. D., Xue, S., Jiang, C., Qiu, G. T., *et al.* (2023) Fatty acids in cancer: metabolic functions and potential treatment. *Medcomm-Oncol.* **2**. https://doi.org/10.1002/mog2.25
33. Pretto, S., Yu, Q., Bourdely, P., Trusso Cafarello, S., Van Acker, H. H., Verelst, J., *et al.* (2025) A functional single-cell metabolic survey identifies Elovl1 as a target to enhance CD8(+) T cell fitness in solid tumours. *Nat. Metab.* **7**, 508–530
34. Zhang, Y., Pang, S., Sun, B., Zhang, M., Jiao, X., Lai, L., *et al.* (2022) ELOVLs predict distinct prognosis value and immunotherapy efficacy in patients with hepatocellular carcinoma. *Front. Oncol.* **12**, 884066